galaxies

MDPI

Review

IXPE View of BH XRBs during the First 2.5 Years of the Mission

Michal Dovčiak [1,*], Jakub Podgorný [1], Jiří Svoboda [1], James F. Steiner [2], Philip Kaaret [3], Henric Krawczynski [4], Adam Ingram [5], Vadim Kravtsov [6], Lorenzo Marra [7,8], Fabio Muleri [9], Javier A. García [10,11], Guglielmo Mastroserio [12], Romana Mikušincová [9], Ajay Ratheesh [9] and Nicole Rodriguez Cavero [4]

1 Astronomical Institute of the Czech Academy of Sciences, Boční II 1401, 14100 Praha, Czech Republic
2 Center for Astrophysics | Harvard & Smithsonian, 60 Garden St, Cambridge, MA 02138, USA
3 NASA Marshall Space Flight Center, Huntsville, AL 35812, USA
4 Physics Department and McDonnell Center for the Space Sciences, Washington University, St. Louis, MO 63130, USA
5 School of Mathematics, Statistics, and Physics, Newcastle University, Newcastle upon Tyne NE1 7RU, UK
6 Department of Physics and Astronomy, University of Turku, 20014 Turku, Finland; vakrau@utu.fi
7 Dipartimento di Fisica e Astronomia, Università degli Studi di Padova, Via Marzolo 8, 35131 Padova, Italy
8 Dipartimento di Matematica e Fisica, Università degli Studi Roma Tre, Via della Vasca Navale 84, 00146 Roma, Italy
9 INAF Istituto di Astrofisica e Planetologia Spaziali, Via del Fosso del Cavaliere 100, 00133 Roma, Italy; fabio.muleri@inaf.it (F.M.)
10 X-ray Astrophysics Laboratory, NASA Goddard Space Flight Center, Greenbelt, MD 20771, USA
11 Cahill Center for Astronomy and Astrophysics, California Institute of Technology, Pasadena, CA 91125, USA
12 Dipartimento di Fisica, Università Degli Studi di Milano, Via Celoria, 16, 20133 Milano, Italy
* Correspondence: dovciak@asu.cas.cz

Abstract: Accreting stellar-mass black holes represent unique laboratories for studying matter and radiation under the influence of extreme gravity. They are highly variable sources going through different accretion states, showing various components in their X-ray spectra from the thermal emission of the accretion disc dominating in the soft state to the up-scattered Comptonisation component from an X-ray corona in the hard state. X-ray polarisation measurements are particularly sensitive to the geometry of the X-ray scatterings and can thus constrain the orientation and relative positions of the innermost components of these systems. The *IXPE* mission has observed about a dozen stellar-mass black holes with masses up to 20 solar masses in X-ray binaries with different orientations and in various accretion states. The low-inclination sources in soft states have shown a low fraction of polarisation. On the other hand, several sources in soft and hard states have revealed X-ray polarisation higher than expected, which poses significant challenges for theoretical interpretation, with 4U 1630–47 being one of the most puzzling sources. *IXPE* has measured the spin of three black holes via the measurement of their polarisation properties in the soft emission state. In each of the three cases, the new results agree with the constraints from the spectral observations. The polarisation observations of the black hole X-ray transient Swift J1727.8–1613 across its entire outburst has revealed that the soft-state polarisation is much weaker than the hard-state polarisation. Remarkably, the observations furthermore show that the polarisation of the bright hard state and that of the 100 times less luminous dim hard state are identical within the accuracy of the measurement. For sources with a radio jet, the electric field polarisation tends to align with the radio jet, indicating the equatorial geometry of the X-ray corona, e.g., in the case of Cyg X–1. In the unique case of Cyg X–3, where the polarisation is perpendicular to the radio jet, the *IXPE* observations reveal the presence and geometry of obscuring material hiding this object from our direct view. The polarisation measurements acquired by the IXPE mission during its first 2.5 years have provided unprecedented insights into the geometry and physical processes of accreting stellar-mass black holes, challenging existing theoretical models and offering new avenues for understanding these extreme systems.

Keywords: X-ray polarisation; high-energy processes; black holes; X-ray binaries

Citation: Dovčiak, M.; Podgorný, J.; Svoboda, J.; Steiner, J.F.; Kaaret, P.; Krawczynski, H.; Ingram, A.; Kravtsov, V.; Marra, L.; Muleri, F.; et al. *IXPE* View of BH XRBs during the First 2.5 Years of the Mission. *Galaxies* **2024**, *12*, 54. https://doi.org/10.3390/galaxies12050054

Academic Editor: Margo Aller

Received: 31 July 2024
Revised: 14 September 2024
Accepted: 20 September 2024
Published: 25 September 2024

1. Introduction

Currently, there are ten known persistent black hole X-ray binaries (BH XRBs) and more than 70 transient ones, see, e.g., [1,2] or their updated catalogue of known BH XRBs at https://www.astro.puc.cl/BlackCAT[1] accessed on 24 September 2024. The latter are in quiescence most of the time but undergo outbursts—periods of increased activity that can last days, weeks, or months. Among these, only slightly more than a dozen transient BH XRBs have experienced at least two outbursts since the birth of X-ray astronomy. Most of the BH XRBs evolve through a well-defined sequence of spectral-timing properties over the course of an outburst see, e.g., [3].

The outburst of a BH XRB outlines a typical q-shaped (turtle head) silhouette in the hardness-intensity diagram (HID), as described by [4,5]. These outbursts usually start in the hard state (HS), where the source abruptly increases in intensity, followed by a transition to the soft state (SS), along the way passing through hard and soft intermediate states (HIMS and SIMS). The HS is characterised by power-law-like Comptonised emission from a corona of hot electrons and the presence of a radio jet [4]. In contrast, the SS is dominated by the thermal multicolour black-body emission of the accretion disc [6,7]. The cycle concludes with a reverse transition from the SS to the HS, which typically occurs at a much lower intensity [8]—sometimes by more than two orders of magnitude—before the source returns to quiescence. During their stay in the SS, many sources also make an excursion to a steep power-law (SPL) state [9].

This general behaviour is thought to be governed by the rate at which the BH is fed material from its donor companion star. If the material is abundant, it may create an envelope made of winds from the accretion disc, behind which the BH may hide itself, see, e.g., [6,10–12]. For instance, the persistent BH XRB GRS 1915+105 obscured itself with accreting material in 2018 [13], and has been hardly visible in X-rays since then.

While the X-ray spectral and timing properties of BH XRBs have been studied extensively in the past, the X-ray polarisation properties of these sources have been, until recently, unknown, with the exception of Cyg X–1 and Cyg X–3 sources, where the first X-ray polarimetric observations were accomplished in the late 1970s by the *OSO–8* satellite, see, e.g., [14]. These early observations, however, performed at 2.6 and 5.2 keV, did not lead to highly significant polarisation detections. More recently, at very high X-ray energies above 130 keV, the *INTEGRAL* mission began to be used to measure polarisation [15], although the mission was not originally constructed or calibrated for this purpose. Even more recently, the *AstroSat* mission was launched, which was designed to offer polarisation capabilities above 100 keV [16].

To study BH XRBs, their journey across the HID, and their polarimetric properties in different accretion states, the medium X-ray energy band (around 1 to 10 keV) is more suitable. At these energies, both the polarisation of SS thermal emission and HS Comptonised coronal emission can be studied, providing further insights into these systems and the physical processes occurring within them. On the one hand, the polarisation observations of the SS in the medium X-ray energy band can help estimate the BH spin [17–20]. On the other hand, in the HS, they can reveal the geometry of the corona [21–23].

The Imaging X-ray Polarimetry Explorer (*IXPE*) mission [24], launched by NASA and ASI in December 2021, is an X-ray mission with polarimetric capabilities. It is sensitive in the 2–8 keV energy band, with an energy resolution of $<$1 keV at 6 keV. Its field of view (FoV) is square with 12.9 arcmin sides, while its angular resolution is $<$30 arcseconds. Thus, for a source at a distance of 10 kpc, *IXPE* sees emission from approximately 40 pc away from the central point of the FoV with a resolution of about 1 pc. The imaging capabilities of *IXPE* were used, for example, in the observation of the Eastern lobe of SS 433 [25]. The limited angular resolution of *IXPE* means that, for a 10 solar-mass ($M_\odot$) BH at a distance of 10 kpc, anything closer than approximately 1 pc, or approximately $10^{12}\,r_\mathrm{g}$, will be confused with the emission coming from the inner parts of these systems. Here, the gravitational radius $r_\mathrm{g} = GM/c^2$, which is 14.8 km for a 10 $M_\odot$ BH. Thus, to correctly identify the origin of polarisation in these sources, spectral decomposition into different

physical components is vital, for example, to estimate the possible contribution from a jet in the HS of these sources.

According to [26], the orbital time of the material in Keplerian orbit around a BH may be expressed in physical units of kiloseconds (ks) as:

$$T_{\rm orb} = 31 \times (r^{2/3} + a) \frac{M}{M_\odot} \frac{\rm ks}{10^9}, \quad (1)$$

where r denotes the orbital radius in units of $r_{\rm g}$, a denotes a dimensionless BH spin parameter ($a \equiv cJ/GM^2$), and M denotes the BH mass. Thus, one Keplerian orbit of the inner accretion disc around a $10\,M_\odot$ BH at $10\,r_{\rm g}$ corresponds to approximately 10 ms. This means that a 10 ks observation of these sources registers photons emitted during one million orbits of the matter at this radius. Given the high photon demand of X-ray polarisation measurements[2], typical exposure times of *IXPE* observations of BH XRBs last for a few tens to a few hundreds of ks to achieve statistically significant detection of polarisation properties[3]. Therefore, almost any variations of polarisation on inner-accretion-disc orbital timescales is lost, even if *IXPE* observations are divided into several time bins. The only exception is the case of (quasi)periodic variability when one may add up photons corresponding to the same phases.

In this paper, we summarise all the observations of BH XRBs performed by *IXPE* during the first 2.5 years of its mission (see Figure 1). The paper is arranged as follows: we describe the data and methods used in Section 2, summarise all *IXPE* BH XRB observations in Section 3, discuss the *IXPE* contribution to the understanding of BH XRBs in Section 4, and finally accentuate the importance of future spectropolarimetric observations in Section 5.

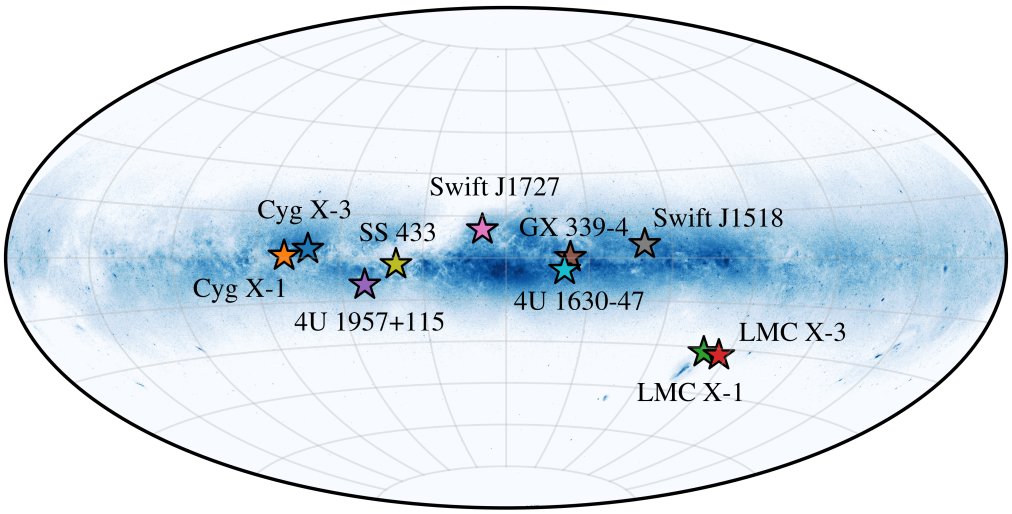

Figure 1. All BH XRBs observed by *IXPE* during the first 2.5 years of its mission. Background image credit: [27], inverted.

2. *IXPE* Data Reduction

While the main advantage of the *IXPE* mission lies in its polarisation capabilities, including imaging[4], the energy resolution is not as good (≈1 keV at 6 keV) as that of other X-ray missions. It also operates over a restricted energy band (2–8 keV). Thus, coordinated parallel observations with other X-ray missions or instruments, such as NICER [28], *Nustar* [29], *XRISM* [30], *Integral* [31], *Swift* [32], etc., are important for determining the source state and spectral properties in more detail. These properties include the amount of absorption, the temperature of the accretion disc, the iron line properties, and the power-law index of the Comptonised component. Such observations are also crucial for estimating the

flux contribution of each spectral component in the *IXPE* energy band, and thus also their possible contribution to the measured polarisation properties. Additionally, MAXI [33] has proved to be a very helpful tool for planning and scheduling *IXPE* observations in particular spectral states.

In various articles on *IXPE* observations, different data reduction and analysis approaches have been used, either with the `ixpeobssim` software [34] or the `heasoft` package [35], in various software versions. Furthermore, the *IXPE* response matrices have been updated several times since the start of the mission. The reduction process also slightly depends on the choices made by the data analyser, such as the selection of source and background regions. Although all these reduction processes yield consistent results if properly done, we have decided to re-analyse for this paper all the available *IXPE* data sets in a uniform manner for better comparison. In some cases, the polarisation degree (PD) has not been published for all data sets (e.g., Cyg X–1, which has an ongoing 2024 campaign), or the results have not been published yet (e.g., Swift J151857.0–572147, where the publication is in preparation).

All data from *IXPE* observations are publicly available at the High Energy Astrophysics Science Archive Research Center (HEASARC)[5]. We have used Level 2 data sets with the source region defined in `SAOimageDS9` v8.3 as a circle around the source centroid with a 100 arcsec radius. Where needed, i.e., where the background could significantly contribute to the spectra, especially at high energies, we have also subtracted the background. In these cases, the background was extracted from an annulus centred on the source, with inner and outer radii of 240 arcsec and 300 arcsec. This was done for LMC X–1, LMC X–3, 4U 1957+11, and for dim states of Swift J1727.8–1613. Regarding *IXPE* background subtraction, see also [36]. Further, in the case of the main HS observation of Cyg X–1 in 2022 and the SS observations in 2023, we have used additional procedures (post-reconstruction calibration of the energy scale and rejection of excess of events at high energies), as described in [37], https://heasarc.gsfc.nasa.gov/FTP/ixpe/data/obs/01/01002901/README accessed on 24 September 2024,and [38], respectively.

The extraction of all three Stokes parameters for both the source and the background was performed using the `xselect` tool from `heasoft` v6.33.2 with simple weighting (i.e., `extract "SPECT" stokes=SIMPLE` was used). The most up-to-date v13 *IXPE* responses from 28 February 2024 were used (see https://heasarc.gsfc.nasa.gov/docs/ixpe/caldb/ accessed on 24 September 2024). The correct *IXPE* `arf` and `mrf` response files were computed with the `ixpecalcarf` tool. Responses for the grey filter were used for the bright HIMS of Swift J1727.8–1613, where the observations were performed with this filter. The computation of responses in this way failed for LMC X–1[6]. Therefore, we adopted an alternate approach for analysing LMC X–1. For this source, we used `ixpeobssim` v31.0.1 with `PHA1`, `PHA1Q`, and `PHA1U` algorithms with the default (`NEFF`) weighting using the `ixpeobssim` v13 responses corresponding to the date of the LMC X–1 observation, i.e., `obssim20220702_alpha075`.

In this way, the energy-dependent Stokes parameters in the original 150 energy channels were created. To compute the polarisation degree and angle in specific energy ranges—either the full *IXPE* 2–8 keV band or for several energy bins—we produced unfolded energy Stokes parameters I, Q, and U, together with their respective errors, using a constant unit model[7] in `XSPEC` v12.14.0h. For each energy range, the Stokes parameters were summed, and the PD and polarisation angle (PA) were computed according to the approach used by [40–42].

To contextualise the *IXPE* observations within their position in the HID, thereby showing their state during the observation[8], we used the MAXI on-demand service [33]. To show the position in the HID, we used MAXI data from the first to the last date of each *IXPE* observation, or else interpolated from the nearest available MAXI data point if no MAXI data were available for the entire duration of an *IXPE* observation. These are denoted by stars in Figures 2 and 3. In these figures, we also show historical positions in the HID for the period between 15/8/2009 and 1/6/2024 (for Cyg X–3 until 17/6/2024),

with three-day time bins shown in the background and coloured grey, except for LMC X–1, LMC X–3, and 4U 1957+11, which are shown in red, blue, and brown, respectively.

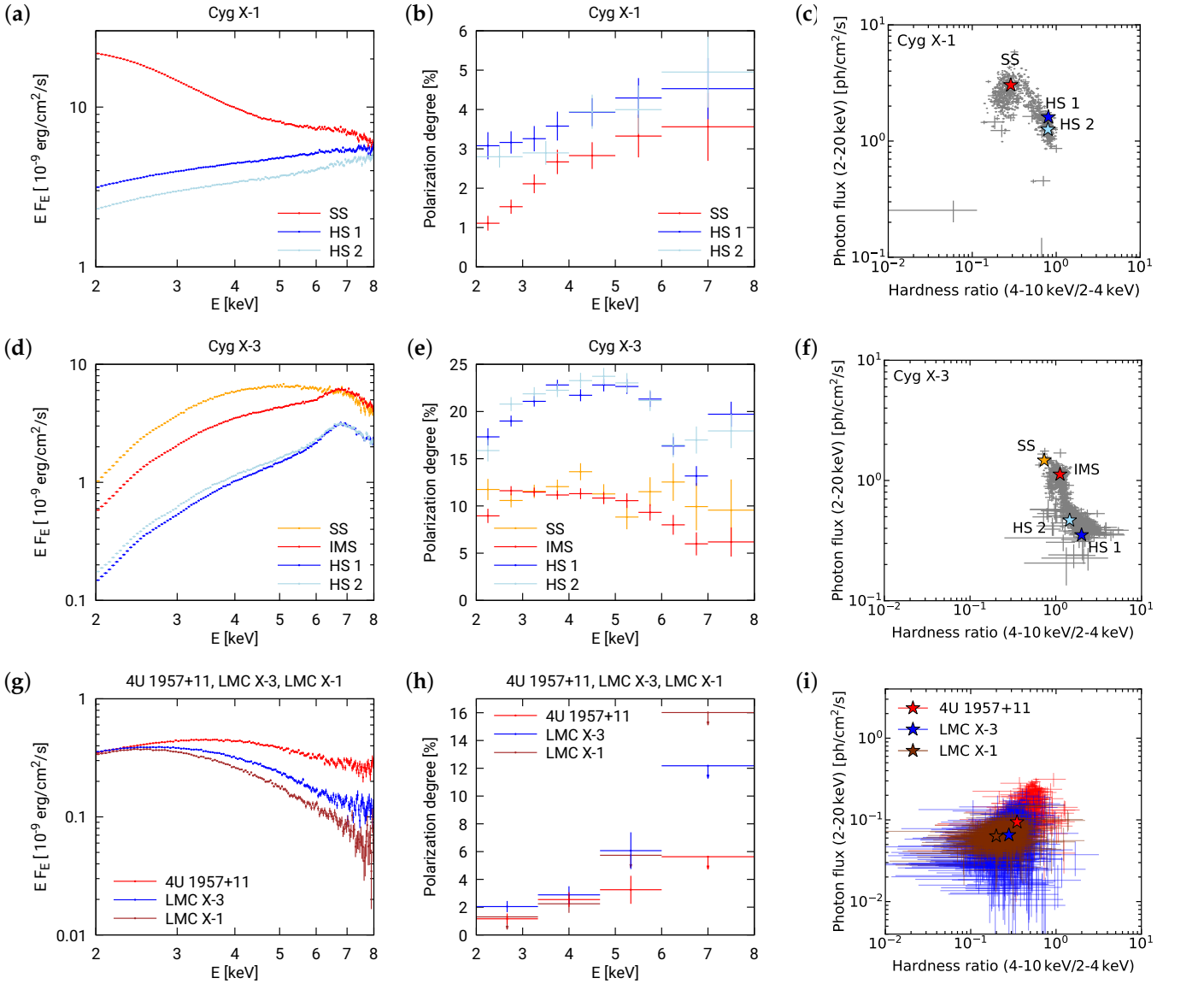

Figure 2. Summary of *IXPE* observations of persistent sources: (**a**) unfolded spectra, (**b**) polarisation degree, and (**c**) position in the MAXI q-diagram for a sum of multiple SS observations (red) and two sets of multiple HS observations (blue and light blue) of Cyg X–1; (**d**) unfolded spectra, (**e**) polarisation degree, and (**f**) position in the MAXI q-diagram for SS (orange), IMS (red), and two HS observations (blue and light blue) of Cyg X–3; and (**g**) unfolded spectra, (**h**) polarisation degree, and (**i**) position in the MAXI q-diagram for SS of 4U1957+11 (red), LMC X–3 (blue), and LMC X–1 (brown). Note that, in the PD energy dependence for 4U 1957+11 and LMC X–3, the observation yielded only an upper limit in the highest energy bin (6–8 keV), while, for LMC X–1, upper limits were obtained in all but the second energy bin.

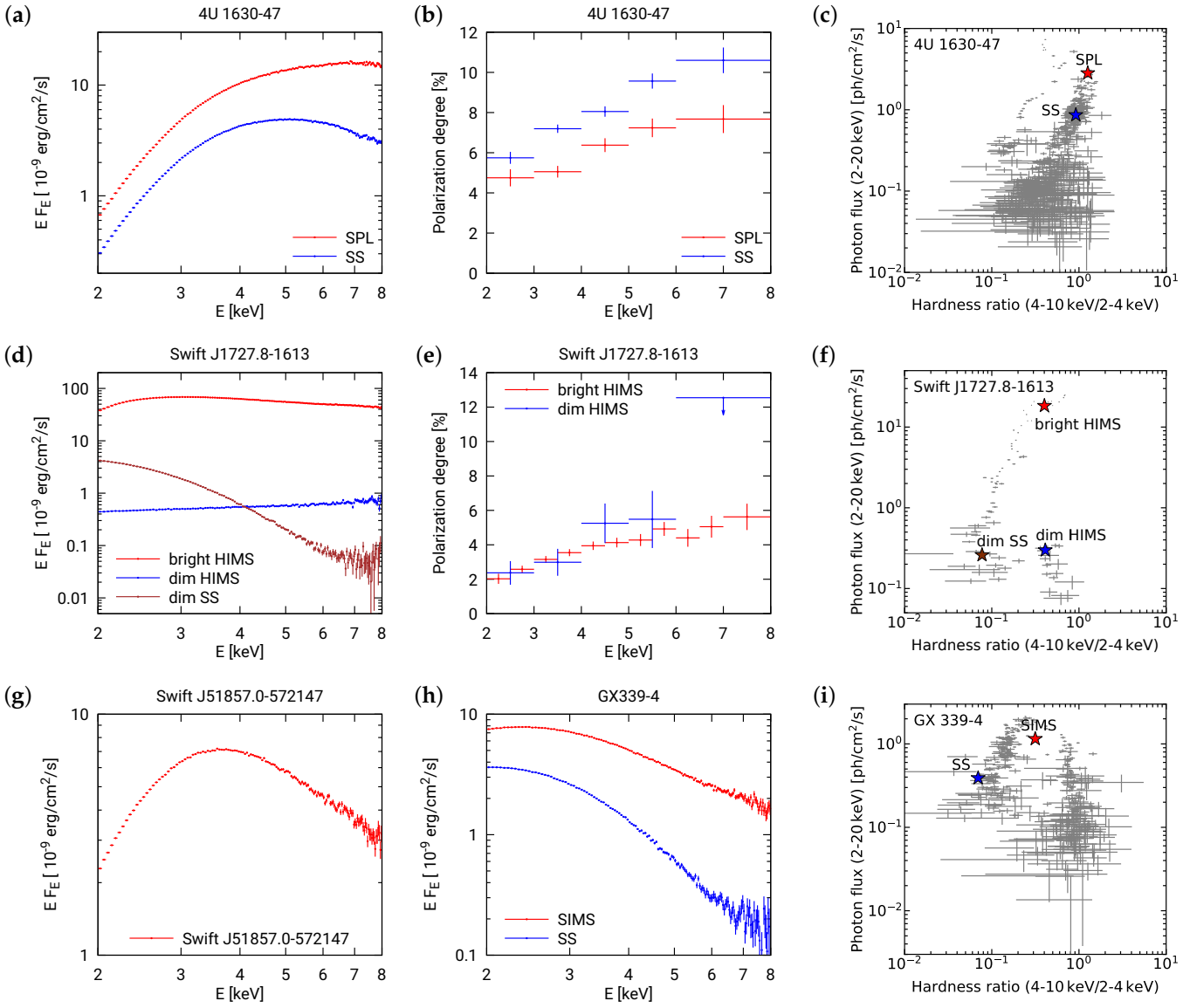

Figure 3. Summary of *IXPE* observations of transient sources: (**a**) unfolded spectra, (**b**) polarisation degree, and (**c**) position in the MAXI q-diagram for SPL state (red) and SS (blue) of 4U1630–47; (**d**) unfolded spectra, (**e**) polarisation degree, and (**f**) position in the MAXI q-diagram for bright HIMS (red), dim HIMS (blue), and dim SS (brown) of Swift J1727.8–1613; (**g**) unfolded spectra of Swift J151857.0–572147 SS (red); (**h**) unfolded spectra of GX 339–4 SIMS (red) and SS (blue), and (**i**) position in MAXI q-diagram for *IXPE* observations of GX 339–4. Note that the energy dependence of the polarisation degree of Swift J1727.8–1613 in dim SS, Swift J151857.0–572147, and GX 339–4 are not shown here since the *IXPE* observations gave only upper limits. The MAXI q-diagram for Swift J151857.0–572147 could not be created (even with on-demand service) due to contamination of the MAXI observation by nearby X-ray source Cir X–1. Since MAXI data are unavailable during and around the *IXPE* observation of SIMS of GX 339–4, we show a point re-scaled from NICER observations, as presented in [43], on the MAXI q-diagram for this source.

3. Summary of *IXPE* Observations of BH XRBs

In this section, we summarise all *IXPE* observations of BH XRBs performed from the beginning of the *IXPE* mission until the end of June 2024; see also the review for the first year of *IXPE* observations [44]. These mainly comprise observations from the prime phase of the mission, but also include observations from Cycle 1 of the *IXPE* General Observer (GO) programme. These GO observations include the dim SS and dim HIMS observations of Swift J1727.8–1613, the SIMS and SS observations of GX 339–4, part of the

observational campaign of Cyg X–1, a Director's Discretionary Time (DDT) observation of Swift J151857.0–572147, and a DDT observation of Cyg X–3 SS. Up to now, *IXPE* has observed five persistent and four transient BH XRBs as point sources, and one extended source—the eastern lobe of SS 433. These sources have been observed over a total of 32 separate observations, with an overall cleaned exposure time (referred to as livetime in the *IXPE* mission) of 5.7 Ms.

The results, reduced as described in the previous section, for persistent sources are summarised in Table 1 and visualised in Figure 2, while the results for transient sources are in Table 2 and Figure 3. We briefly describe the basic results for each source in the following subsections. Note that the source properties are taken from the original *IXPE* collaboration papers, where the references are given for each basic system property (distance, inclination, BH mass and spin, etc.) unless directly referred to in this paper.

Table 1. Basic information for all *IXPE* observations of persistent BH XRBs performed until June 2024. The energy flux, polarisation degree, and angle for the full length of observation, given by livetime in the full *IXPE* energy band of 2–8 keV, are provided except where stated otherwise. All errors are presented at 1σ significance level. See the text for details on the data reduction process.

Object (Object Type)	Observation Date	LIVETIME [ks]	State	Energy Flux [a] [mCrab]	Polarisation Degree [a] [%]	Polarisation Angle [a] [deg]	Ref. [b]
Cyg X–1 [c] persistent HMXB	15–21 May 2022	242	HS 1 [d]	238	4.1 ± 0.2	-22 ± 2	[37]
	18–20 June 2022	86		273	3.6 ± 0.4	-24 ± 3	[37]
	2–3 May 2023	21	SS [e]	515	2.6 ± 0.4	-13 ± 5	[38]
	9–10 May 2023	31		632	2.8 ± 0.3	-23 ± 3	[38]
	24–25 May 2023	25		689	2.3 ± 0.3	-18 ± 4	[38]
	13–14 June 2023	29		677	1.6 ± 0.3	-15 ± 6	[38]
	20 June 2023	35		895	1.9 ± 0.3	-31 ± 4	[38]
	12–13 April 2024	56	HS 2 [f]	203	4.2 ± 0.6	-30 ± 4	
	6–7 May 2024	54		220	3.0 ± 0.6	-15 ± 5	
	26–27 May 2024	58		207	4.0 ± 0.5	-25 ± 4	
	14–15 June 2024	56		166	4.3 ± 0.6	-30 ± 4	
Cyg X–3 [g] persistent HMXB	14 October–6 November 2022	538	HS 1	72	19.5 ± 0.4	89.9 ± 0.5	[45]
	17–23 November 2023	291	HS 2	76	20.0 ± 0.5	91.8 ± 0.7	
	25–29 December 2022	198	IMS	192	9.3 ± 0.3	92 ± 1	[45]
	2–3 June 2024	50	SS	268	11.3 ± 0.5	93 ± 1	[46]

Table 1. *Cont.*

Object (Object Type)	Observation Date	LIVETIME [ks]	State	Energy Flux [a] [mCrab]	Polarisation Degree [a] [%]	Polarisation Angle [a] [deg]	Ref. [b]
LMC X–1 persistent HMXB	19–28 October 2022	562	SS	14	< 2.5 [h]	—	[47]
LMC X–3 persistent LMXB/HMXB	7–20 July 2023	562	SS	16	3.0 ± 0.4	-41 ± 4	[48]
4U 1957+11 persistent LMXB	12–24 May 2023	572	SS	22	1.8 ± 0.4	-52 ± 7	[49]

[a] The source energy flux, PD, and PA are computed from the unfolded Stokes parameters (using "eufs" in `XSPEC`) in the original energy binning, which were summed in the 2–8 keV band across all three detectors. [b] The references in this table refer to the papers by the *IXPE* collaboration; references to other works published on these sources are cited in the text. [c] The PA in all states observed by *IXPE* is consistent with the radio jet direction. [d] The sum of these observations gives PD = (3.9 ± 0.2)% and PA = $-23^\circ \pm 2^\circ$. [e] The sum of these observations gives PD = (2.2 ± 0.1)% and PA = $-21^\circ \pm 2^\circ$. [f] The sum of these observations gives PD = (3.8 ± 0.3)% and PA = $-25^\circ \pm 2^\circ$. [g] The polarisation direction in all states observed by *IXPE* is consistent with being perpendicular to the direction of radio ejections. [h] The upper limit is given at the 99% confidence level and is computed from the result of PD=(1.3 ± 0.5)% and PA = $62^\circ \pm 10^\circ$.

Table 2. Basic information for all *IXPE* observations of transient BH XRBs performed until June 2024. The energy flux, polarisation degree, and angle for the full length of observation, given by livetime in the full *IXPE* energy band of 2–8 keV, are provided except where stated otherwise. All errors are presented at 1σ significance level. See the text for details on the data reduction process.

Object (Object Type)	Observation Date	LIVETIME [ks]	State	Energy Flux [a] [mCrab]	Polarisation Degree [a] [%]	Polarisation Angle [a] [deg]	Ref. [b]
4U 1630–47 transient LMXB	23 August 2022 – 2 September 2022	458	SS	181	8.6 ± 0.2	17.6 ± 0.6	[50]
	10–13 March 2023	36 102	SPL [c]	389 539	8.3 ± 0.5 6.7 ± 0.3	22 ± 2 21 ± 1	[51]
Swift J1727.8–1613 [d] transient LMXB	7–8 September 2023	19	bright HIMS [e]	3920	4.1 ± 0.2	3 ± 2	[52]
	16–17 September 2023	37		3574	3.9 ± 0.2	3 ± 1	[39]
	27–28 September 2023	21		3050	3.7 ± 0.2	3 ± 2	[39]
	4 October 2023	18		3284	3.2 ± 0.2	0 ± 2	[39]
	10 October 2023	18		2676	2.8 ± 0.3	-1 ± 3	[39]

Table 2. *Cont.*

Object (Object Type)	Observation Date	LIVETIME [ks]	State	Energy Flux [a] [mCrab]	Polarisation Degree [a] [%]	Polarisation Angle [a] [deg]	Ref. [b]
Swift J1727.8–1613 [d] transient LMXB	11–12 February 2023	67	dim SS [f]	86	<1.1	—	[53]
	20–23 February 2023	151		58			
	3–8 April 2023	202	dim HIMS	32	4.0 ± 0.7	6 ± 5	[54]
GX 339–4 [g] transient LMXB	14–16 February 2024	95	SIMS	291	1.3 ± 0.4 [h]	-69 ± 8 [h]	[43]
	8–10 March 2024	98	SS	94	<1.4 [i]	—	[43]
Swift J151857.0–572147 transient BHC	18–20 March 2024	96	SS	300	<1.3 [j]	—	García et al., in preparation

[a] The source energy flux, PD, and PA are computed from the unfolded Stokes parameters (using "eufs" in `XSPEC`) in the original energy binning, which were summed in the 2–8 keV band across all three detectors. [b] The references in this table mostly refer to papers by the *IXPE* collaboration; references to other works published on these sources are cited in the text. [c] The observation was split into two with different average flux levels. The full observation gives PD = (7.0 ± 0.2)% and PA = $21^\circ \pm 1^\circ$. [d] The polarisation direction in the HIMS is consistent with the radio jet direction. [e] The observations were performed with the grey filter. The sum of these observations gives PD = (3.6 ± 0.1)% and PA = $1.9^\circ \pm 0.8^\circ$. [f] The two dim SS observations were combined to provide a stronger upper limit. The upper limit is given at the 99% confidence level and is computed from the result of PD = (0.42 ± 0.27)% and PA = $1^\circ \pm 22^\circ$. [g] The polarisation direction in the SIMS is consistent with the direction of the ballistic radio jet. [h] The result is for 3–8 keV energy band. The 2–8 keV band gave only an upper limit of 1.3% (at the 99% confidence level) computed from the result of PD = (0.67 ± 0.24)% and PA = $-68^\circ \pm 11^\circ$. [i] The upper limit is given at the 99% confidence level and is computed from the result of PD = (0.50 ± 0.34)% and PA = $-37^\circ \pm 23^\circ$. [j] The upper limit is given at the 99% confidence level and is computed from the result of PD = (0.51 ± 0.28)% and PA = $-32^\circ \pm 18^\circ$.

3.1. Cyg X–1

Cyg X–1 is the first identified and brightest persistent BH XRB in our Galaxy, with the X-ray flux varying between 0.2 and 2 Crab ($\approx$0.5 to 5 $\times 10^{-8}$ erg/s/cm^2). The system is located at a distance of 2.2 kpc and consists of a $20 M_\odot$ BH and $40 M_\odot$ O-supergiant companion [55]. The binary inclination is constrained to be 27° [56]. Previous analyses of the thermal continuum and the shape of the X-ray emission lines have indicated that the BH in Cyg X–1 spins rapidly, see, e.g., [57,58]. The first X-ray polarisation measurements of Cyg X–1 by the *OSO–8* mission were reported in [14]. Cyg X–1 thus became the first BH target for *IXPE* in May 2022, and since then it has been the most frequently observed BH XRB, with multiple exposures in different accretion states (see Table 1).

Already, the first observations in the HS have provided spectacular results. The PA was found to be perfectly aligned with the radio jet. Because the resulting polarisation should have the direction perpendicular to the scattering plane, this measurement showed a clear preference for an equatorially extended X-ray corona rather than a lamp-post geometry [37]. The measured PD $\approx$ 4% was higher than expected from the low inclination angle (but consistent with the archival *OSO–8* measurements). To explain this relatively high polarisation fraction, a higher inclination of the innermost accretion disc [37] or an outflowing corona [59,60] were proposed. The PD was also found to increase with the energy, which was later observed in several other sources as well.

The Cyg X–1 observations in SS[9] revealed a significant decrease in the PD, which dropped to 2% [62,63], while the polarisation direction and the energy dependence remained preserved [38]. The polarisation signal is best explained by models with extremely high spin ($a > 0.96$) and albedo (reflectivity of the disc surface), for which the reflection of the returning radiation prevails in the polarisation signal and shapes the resulting PD and PA [38].

3.2. Cyg X–3

Cyg X–3 is a persistent HMXB located at a distance of approximately 9 kpc [64]. The mass of the compact object in this system is estimated to be low [65], and thus a neutron star cannot be ruled out. Its radio, infrared, and X-ray properties, however, classify it as a BHC [66]. Its companion on a very close orbit (orbital period approximately 4.8 h) is a massive Wolf–Rayet star producing strong winds [67]. Spatially resolved discrete radio ejections are observed in this system in the north–south direction [68]. The system has ≈30° inclination [69]. X-ray polarisation observations of this object were performed for the first time by the *OSO–8* satellite [14] with a PD ≈ 10% at 2.6 keV and with a polarisation direction in a roughly east–west direction on the sky. However, the measurement had a low statistical significance.

IXPE has observed this source several times—twice in the HS (observations in autumn 2022 and 2023), once in the IMS (observation in late 2022), and once in the SS (spring 2024). The 2022 observations are reported in the *IXPE* collaboration paper [45], and the SS observations in 2024 are presented in [46] and in Rodriguez Cavero et al., in preparation. In all of these observations, very high levels of polarisation were measured, with the direction perpendicular to the motion of the radio ejections. While the PD in the HS was ≈20%, it was about half of that value in the IMS and the SS. Such high PDs can be explained if the direct emission, which has a much lower polarisation level, is obscured by dense material, likely an optically thick wind emanating from the accretion disc. This material forms a narrow cone around the BH, allowing the observer to see only the reflection from the walls of this cone. The reflected X-rays are highly polarised perpendicularly to the cone axis, which therefore must coincide with the direction of radio ejections. The lower level of polarisation in the IMS and the SS is then explained if the cone is filled with lower-density and more highly ionised material [46] or if the reflecting material of the cone itself is more highly ionised (Rodriguez Cavero et al., in preparation).

3.3. LMC X–1

LMC X–1 is a persistent HMXB located in the Large Magellanic Cloud at a distance of 50 kpc [70], with a BH mass of $\approx 11\,M_\odot$ and an orbital inclination of 36° [71]. In the past, a high BH spin parameter, $0.85 \lesssim a \lesssim 0.95$ [72], and $0.93 \lesssim a \lesssim 0.97$ [73], has been estimated for this source using the thermal continuum and inner accretion flow line fitting methods, respectively.

IXPE observed this source from 19 to 28 October 2022, in coordination with NICER and *NuSTAR*. The source was found in its typical SS. The observation provided an upper limit on the PD of 2.2% at a 3σ confidence level [47], which was relatively high due to the system's low flux. This result is consistent with the polarisation level expected for a standard thermal disc with a low inclination.

3.4. LMC X–3

The *IXPE* observation of this source is described in detail in an *IXPE* collaboration paper [48], as well as in [74,75]. This system is located at a distance of 50 kpc in the Large Magellanic Cloud, has an inclination of 69°, and harbours a BH with a mass of $7\,M_\odot$ [76]. The BH spin has been measured with the thermal X-ray continuum to be $a \approx 0.2$ [48,77] or $a \approx 0.1$ [78].

IXPE observed the source in the SS with a very small contribution from the Comptonised component. The observed PD is consistent with that of a standard accretion disc.

Its rather high value (2 to 3%) at low energies (2–4 keV) and no significant rotation of the PA with energy constrains the BH spin to be low, $a \approx 0.2$. The orientation of the system on the sky is not known since no radio jets, ionisation cones, or similar structures that could indicate the direction of the system axis have been observed. Assuming the direction of polarisation to be parallel with the disc (as is expected for a low-spinning BH system), the system position angle is ≈47° to the east from the north.

3.5. 4U 1957+11

Despite being one of the few historically persistently active BHCs, there is limited information available about the system's mass, distance, and inclination. The observed orbital variability in optical emission suggests that the total mass of the binary system is relatively low ($\lesssim 6\,M_\odot$). This is consistent with the compact object being either a neutron star or a low-mass BH. However, the absence of Type I bursts, pulsations, surface emission components, or boundary layer emission signatures in the X-ray spectra disfavours the neutron star hypothesis. Modelling of interstellar medium absorption indicates that the source is located outside the galactic plane, at a distance of at least 5 kpc. The lack of eclipses and orbital modulations in the X-ray light curve combined with optical variability modelling provide an upper limit for the system's inclination of 75°. Various estimates of 4U 1957+11's spin, derived from analysing the reflection component and fitting the continuum of the disc component, consistently describe the source as rapidly rotating.

The *IXPE* observations of 4U 1957+11 have been described in detail in [49]. The spectropolarimetric fit of the combined *IXPE*, NICER, and *NuSTAR* observations prefers a rather high inclination of $\gtrsim 50°$ and very high BH spin of $a \gtrsim 0.96$. The high spin is favoured due to the increase in the PD with energy in combination with a low PD of ≈1.2% at low energies below ≈3.3 keV and due to the rotation of the PA by ≈20° moving from lower to higher energies (compared with LMC X–3 where a higher PD and no significant rotation of the PA with energy were observed). This behaviour is expected if a large fraction of disc self-irradiation is reflected towards the observer [19,79]; therefore, a strong disc albedo is predicted in this source. The *IXPE* observations showed that the PD slightly increased during the observation, probably due to the relative decrease of the Comptonised contribution to the emission that reduced the polarisation of the thermal component. Similarly to LMC X–3, the orientation of this source on the sky is unknown. The *IXPE* measurements imply a system axis orientation at ≈70° to the west from north.

3.6. 4U 1630–47

4U 1630–47 is a transient low-mass XRB (LMXB) system exhibiting recurrent outbursts every 2–3 years. The BH mass, distance to the system, and its inclination are poorly constrained. The mass is estimated to be 10 $M_\odot$, the distance is estimated to be 4.7 to 11.5 kpc, while the inclination is believed to be ≈65° (explaining the observations of X-ray dips and the absence of eclipses). The source shows evidence for an equatorial wind. The thermal component usually dominates the spectrum during the outbursts of 4U 1630–47, and thus it is an ideal object to study polarisation properties of the SS in BH XRBs.

IXPE has observed this source in two different states—the SS and the SPL state. The detailed analysis of these observations has been reported in *IXPE* collaboration papers [50,51] as well as in other articles [80–82]. In both states, a very high level of polarisation was measured that increases with energy. The polarisation in the SS (≈8.6%) was higher than in the SPL state (≈6.7%). Such a high PD is incompatible with a standard accretion disc. Since the orientation on the sky is not known for this object, it cannot be determined how the polarisation direction, which was observed to be the same in both states, is aligned relative to the accretion disc. Several scenarios have been suggested to explain the polarisation behaviour in this source, neither of them explaining all the details in a satisfactory manner. An edge-on view of the inner accretion disc misaligned with the orbital plane seems to be the simplest solution [50], while the toy model of outflowing upper layers of the disc (base of magnetohydrodynamic disc winds?) seems too far-fetched due to very high vertical

velocities of high-density disc material required [50]. The similarity of the polarisation properties in the SS and SPL state including the PD decrease could be explained if the same system geometry is preserved, but the scattering mechanism changes from Thomson to inverse Compton (due to more efficient heating of electrons) that naturally produces the observed power-law component and the decrease in the PD in the SPL state. Other proposed explanations, reflection of disc self-irradiation for a geometrically thick disc [50,83] and scattering in the thermal wind [84,85], do not seem to be able to explain the observed polarisation properties.

3.7. Swift J1727.8–1613

The newly discovered black-hole X-ray transient, Swift J1727.8–1613, went through a bright X-ray outburst, reaching an X-ray flux of 7 Crabs ($\approx 1.7 \times 10^{-7}$ erg/s/cm^2) in the 2–20 keV range [86,87]. The distance of the source was measured as $D = 2.7 \pm 0.3$ kpc using optical spectroscopy [88]. Although the BH mass in this source has not been measured yet, its BH nature was confirmed by X-ray spectroscopy and timing analysis. Using X-ray reflection spectra, it was suggested that the BH is rapidly rotating [89].

IXPE observed the source a couple of weeks after its appearance in the X-ray sky and detected a high level of polarisation with a measured PD $\approx$ 4 % [52] and a polarisation direction aligned with the radio jet [90]. The presence of QPO allowed for the first time a polarimetric analysis of QPOs in BH XRBs [91] but no modulation of the PD or the PA was detected in relation to the QPO phase. The following monitoring of the source in the HIMS [39] revealed a slight decrease in the PD (from 4 to 3%), with the source transiting toward the SS. Due to the Sun-angle constraints, *IXPE* observations in the SS were possible only after four months in February 2024 when the source was about two orders of magnitude fainter than during the peak of the outburst. A dramatic reduction in the PD was found with an upper limit on the PD of 1.2% [53]. A remarkable recovery of polarisation properties was detected in the latest *IXPE* observation after the soft-to-hard transition [54]. The PD $\approx$ 3.3% in the dim HIMS is identical to the bright HIMS measurements with the similar X-ray spectral hardness. Similar to the HS of Cyg X–1, the polarisation aligned with the jet indicates that the corona in both the bright and dim HIMS in this source may have a flat geometry in the plane perpendicular to the radio jet. The low PD in the SS is consistent with the standard accretion disc.

3.8. GX 339–4

GX 339–4 is a LMXB with an estimated BH mass of $\approx$4–11 $M_\odot$ and inclination of $\approx$40°–60°. The system is located at a distance of $\approx$8–12 kpc, see, e.g., [92]. In some works, the BH spin for this source has been estimated to be rather high, with $a \gtrsim 0.8$ [93–95], while other studies suggest a low spin of $a \sim 0$ [96,97].

The *IXPE* observed this source twice during Cycle 1 of the *IXPE* GO programme (see Table 2, and (h) and (i) panels in Figure 3). Initially, the source was in the SIMS, while later it was observed in the SS. In 2–8 keV, only an upper limit on the PD could be determined for both observations. However, in the first observation, a PD of $\sim$1.3% in the 3–8 keV range was detected with more than 3σ significance, with the polarisation direction consistent with the motion of the radio ejecta observed with ATCA in May 2024 [43], as well as with the radio ejecta motion observed in 2002 [98]. This suggests that: (i) similar to the *IXPE* observations of different states of Swift J1727.8–1613, this source is less polarised in the SS than during the transition from the HS to the SS, and (ii) the polarisation direction in the SIMS of GX 339–4 aligns with the radio jet, as seen in Cyg X–1 and Swift J1727.8–1613. Furthermore, the first observation hints that the lower energy bin (2–3 keV) may be depolarised due either to the contribution of the soft thermal component or to the contribution of once-scattered photons in the sandwich corona scenario. In both cases, a polarisation direction perpendicular to that of multiple-scattered photons in the sandwich corona, dominant at higher energy bins (above 3 keV), is expected [21]. For the full spectropolarimetric analysis of these observations, see [43].

3.9. Swift J151857.0–572147

This source was first discovered by Swift in early March 2024 [99]. Soon, many other instruments observed this source in various wavelengths, including an X-ray campaign when *IXPE* performed coordinated observations with NICER and *NuSTAR*. At the time of writing of this review, the nature of this Galactic transient has not yet been established and we thus refer to it as a BHC, see [100]. While most of the system properties, like BH mass and system inclination, are yet to be measured, the observation with MeerKAT [101] estimated the distance to this source to be in the range of 4.5–15.6 kpc.

When *IXPE* observed this source from 18 to 20 March 2024, it was already in its SS, since the transition from HS to SS happened around 9–10 March 2024, according to [100,102]. The *IXPE* observation gave a rather low upper limit of 1.3% for the PD, see Table 2. This could also indicate that the source was caught in its SS. The whole *IXPE*, NICER, and *NuSTAR* campaign is analysed in García et al., in preparation.

3.10. Eastern lobe of SS 433

SS 433 is a BHC located at a distance of 5.5 kpc with bipolar jets, with a position angle of 100° and inclination of 80°. These interact with the surrounding supernova remnant, creating two lobes east and west from SS 433. The "Head" region of the eastern lobe, which is the closest to the BH, is characterised by nonthermal hard X-ray emission and thus probably is an acceleration site for high-energy particles, where the kinetic energy of the bulk motion of the flow is transformed into the acceleration of particles. *IXPE* has measured the PD to be in the range of 38% to 77% at the 68% confidence level. The high value of the PD indicates that the magnetic field near the acceleration region has a well-ordered component if the X-ray emission is due to synchrotron radiation. The PA is in the range of $-12°$ to $+10°$ (east of north), which indicates that this component is parallel to the jet. This result places constraints on models of the acceleration process and origin of the magnetic fields in these regions. All the details of this *IXPE* observation are described in the collaboration paper [25].

4. *IXPE* Achievements in Observations of BH XRBs

During the first 2.5 years of its mission, *IXPE* has observed a large variety of BH XRBs—systems have been observed in different states, HS (Cyg X–1), HIMS (Swift J1727.8–1613), SIMS (GX 339–4), SS (Cyg X–1, LMC X–1, LMC X–3, 4U 1957+11, 4U 1630–47, Swift J1727.8–1613, GX 339–4, Swift J151857.0–572147), and SPL state (4U 1630–47). It captured one obscured object (Cyg X–3) in different states (HS, IMS, and SS), and it performed a unique campaign of multiple observations across the HID (Swift J1727.8–1613—five observations during the transition from HS to SS, two observations in the dim SS, and one observation in the reverse transition back to the HS). Finally, imaging capabilities of the *IXPE* have been utilised in observation of the eastern lobe of SS 433. Here, we would like to highlight the most interesting results from these observations.

4.1. Geometry of Corona

One science objective of the *IXPE* mission is to constrain the geometry of the corona in the HS of BH XRBs. During the first 2.5 years, *IXPE* managed to observe three objects in their HS or during their transition to the SS—Cyg X–1 (HS), Swift J1727.8–1613 (HIMS), and GX 339–4 (SIMS). In the first two sources, remarkably similar polarisation properties were observed: the PD was around ≈4% while the polarisation direction was parallel with the radio jet. The latter was also true for GX 339–4.

In Cyg X–1's HS, the orbital inclination of 27° is too low to explain such a large polarisation level with the usually considered coronal geometries. As discussed in [37], possible interpretations of these results include a misalignment of the inner accretion disc relative to the binary orbit [103], or a corona outflowing from the disc with relativistic velocities [59]. In both of these solutions, a flat corona extended in the plane perpendicular

to the radio jet is preferred. The hot inner accretion flow first proposed for Cyg X–1 in [104] could in principle act as such a corona.

The inclination of Swift J1727.8–1613 is not known yet; however, a very low PD observed in its SS may indicate that the inclination of this system is rather low. Thus, it is possible that the corona properties in this source are similar to those observed in Cyg X–1. A very remarkable result of the *IXPE* observation of this source is, however, the gradual decrease of the PD as the source transits from the HS to the SS, a very low PD in its SS, and the re-acquisition of the PD on its reverse transit back to the HS. This indicates that the corona, responsible for the observed Comptonised emission, should have similar geometries in both the bright HIMS at the beginning of the outburst and in the dim HIMS towards the end of the transient outburst.

While the orbital inclination in GX 339–4, estimated to be between 40° and 60°, is higher than that of Cyg X–1, the observed PD was much smaller, at approximately 1.3% in the 3–8 keV range. This could be due to the fact that the source was observed in the SIMS, very close to the SS, as suggested by the decreasing PD trend in the hard-to-soft transition in Swift J1727.8–1613. Additionally, the alignment of the polarisation direction with the ballistic radio jet may suggest the presence of a corona extended perpendicularly to the jet in this source as well.

Polarisation aligned with the jet has also been observed with *IXPE* in two active galactic nuclei (AGN), NGC 4151 [105,106] and IC 4329A [107]; see also the review of *IXPE* observations of radio-quiet AGN in [108]. On one hand, this is not surprising, as BH XRBs are considered to be scaled-down versions of AGN, often referred to as microquasars [109]. On the other hand, while this polarisation alignment has been observed in the HS or IMS of XRBs, in AGN it has been observed in radio-quiet AGN, which are thought to correspond to the SS of XRBs. This could suggest that the corona may have a similar geometry in both the SS and HS.

4.2. BH Spin Measurements

Another prime objectives of the *IXPE* mission is to constrain BH spins via spectral polarimetry of BH XRBs. This is best done by observing in the SS because then the X-ray emission is dominated by the inner regions of the accretion disc, where the gravity of the BH has the strongest effect. This objective has now been accomplished for the first time for LMC X–3, 4U 1957+11, and Cyg X–1. While LMC X–3 and 4U 1957+11 are persistently in the SS, Cyg X–1 is a persistent source that often changes between the HS and SS. All three *IXPE* spin measurements are consistent with those obtained by other methods. *IXPE* has demonstrated a new method to measure BH spin.

For LMC X–3, the PD increases with energy while the PA is consistent with being constant with energy, and a low spin, $a \approx 0.2$, is inferred from spectropolarimetric analysis.

For 4U 1957+11, there is a marginal increase in the PD with energy while the PA rotates by ≈20°, moving from the 2–3 keV bin to higher energies, and a high spin, $a > 0.96$, is preferred.

For Cyg X–1, the PD in the SS increases with energy while the polarisation direction is parallel with the system axis (i.e., consistent with the radio jet present during the HS). This is due to the reflection of returning radiation that is polarised perpendicularly to the accretion disc. The rotation of the PA with energy is not observed in this source. This is due to the accretion rate being rather low[10]. In this case, the polarisation of returning radiation already dominates the one due to the direct thermal emission in the *IXPE* energy band, and the swing in the PA by 90° is expected to happen at lower energies. The polarimetric model prefers high spin, $a > 0.96$.

All the other SS observations gave only an upper limit on the PDs. Given the uncertainty of their inclinations, the polarimetric results did not give hard limits on the BH spins. This was the case for LMC X–1, Swift J1727.8–1613, GX 339–4, and Swift J151857.0–572147, for which *IXPE* merely gave upper limits on the PDs. The PD upper limits can be used to place upper limits on the source inclinations. While the inclination of the newly discovered

transients Swift J1727.8–1613 and Swift J151857.0–572147 has not been constrained by other measurements, LMC X–1 is known to have a rather low orbital inclination of 36°, and GX 339–4 is estimated to have moderate orbital inclinations of 40° to 60°.

4.3. Geometry of the Obscuring Funnel

The *IXPE* observations of Cyg X–3 have confirmed its nature of a source enshrouded by an optically thick material. This material, probably a dense thermal wind from the accretion disc, obscures the inner accretion flow. X-rays can escape the accretion flow through a funnel—presumably along the magnetic axis or spin axis of the compact object—through reflection from the funnel walls or by scattering in the less dense material inside the funnel. As a consequence, a high level of polarisation perpendicular to the cone is observed. The polarisation properties thus mainly depend on the geometry and state of the reflector rather than on the state of the source itself. For this reason, the *IXPE* observations do not constrain the spin of the compact object nor the corona of the inner accretion flow. On the other hand, the *IXPE* observations reveal the nature of this source as a heavily obscured object and constrain the geometry of the obscuring material.

Similarly, a high PD with direction perpendicular to the radio jet or radio structure axis was observed in the case of two Seyfert 2 galaxies observed with *IXPE*: Circinus Galaxy [110] and NGC 1068 [111]; see also the review of *IXPE* observations of radio-quiet AGN in [108]. In both cases, the origin of polarisation is attributed to cold reflection from a distant, optically thick torus with a half-opening angle of $\approx 50°$, which resembles the scenario in Cyg X–3.

4.4. Exceptional Case of 4U 1630–47

As usual with opening a new observational window, some unanticipated results may be acquired. In the case of BH XRBs, the observation of 4U 1630–47 may be considered to be such a case. Specifically, its unexpectedly high polarisation level increasing with energy measured in its SS is hard to explain with the standard model of accretion disc. Thus, further theoretical investigations are needed to satisfactorily explain the processes in this source.

Further interesting findings obtained by the *IXPE* mission worth mentioning are according to us that (i) Cyg X–1 and Cyg X–3, as the only sources that were revisited in the same state (both in the HS) after a year, were found to have very similar polarisation properties, although in between the observations these sources transited to a different state; and (ii) Cyg X–1, the most frequently observed BH XRB by *IXPE*, exhibits some polarisation properties variability in its HS. The former suggests that the spectral and timing properties defining the HS (and obscured HS) of the object are closely connected to the geometry of the corona (and obscuring funnel) in this state, producing the same polarimetric signatures. The latter, on the other hand, suggests that, although the corona keeps a similar general shape in the HS, it still is a dynamical physical component. The reason for this variability should be studied in the future.

5. Future Spectropolarimetric Observations of BH XRBs

Looking forward, it is important for *IXPE* to perform additional observations of BH XRBs in both the SS and HS. One of the brightest BH XRBs in the sky, GRS 1915+105, has been in a heavily absorbed state since *IXPE* was launched [13]. The source would be a prime target for spectropolarimetric studies with *IXPE* should it resume its usual activity. Transients tend to transition from the HS through the SS and back to the HS, and such ToO observations should be prioritised. A large number of statistics will be needed to provide robust constraints on the dependence of the PD and PA on energy. An exciting result would be to measure the rotation of the PA predicted for rapidly-rotating BHs in the SS arising from the rotation of spacetime in strong gravity [17], which would enable the measurement of BH spin in more sources with this new method. It would also be exciting to confirm

that the coronal geometry in the HS is similar in most of the BH XRBs. Such confirmation would provide an important insight into the accretion physics.

The IMS of BH XRBs is marked by increased jet activity and changes in their timing properties [112]. In the past, it was suggested that part of the X-ray emission in XRBs may originate from the jet [113]. While jet-induced polarisation is not favoured for Cyg X–1, it may not be true for all BH XRBs. Some studies have reported changes in coronal geometry during state transitions [114]. In such scenarios, a rotation of the polarisation direction could be expected as the source transits from the HS to the SS. Polarisation observations in the IMS could thus provide valuable insights into changes in the geometrical configuration of corona. Therefore, *IXPE* observations of additional sources as they move through the HID to track their polarisation properties are crucial. There are also unobserved states of BH XRBs, such as the flaring state of Cyg X–3 or the SPL state, which have so far been observed only in the exceptional case of 4U 1630–47. As with any new observations, we can always hope for more surprises along the way, such as the case of 4U 1630–47.

Additional insights will be provided by extending the spectropolarimetric observations of *IXPE* to lower and higher energies. The *XL-Calibur* mission [115], operating at 15–80 keV, observed Cyg X–1 in June 2024, and spectropolarimetric constraints are forthcoming. The *XPoSat*[11] mission was launched on 1 January 2024, carrying the POLIX instrument onboard, which will measure polarisation in the 8–30 keV energy band. The *COSI* mission, set to launch in 2028, promises spectropolarimetric capabilities at energies of a few hundred keV [116]. At the other end, the REDSoX sounding rocket mission will demonstrate the feasibility of X-ray polarimetry in the 0.2–0.4 keV energy range [117]. Extending the bandpass will allow for better disentanglement of the polarisation contributions from different emission components.

Author Contributions: Formal analysis, M.D., J.P. and V.K.; writing—original draft preparation, M.D., J.S., P.K., H.K. and L.M.; writing—review and editing, M.D., J.S., J.F.S., P.K., H.K., A.I., V.K., L.M., F.M., J.A.G., G.M., R.M., A.R. and N.R.C. All authors have read and agreed to the published version of the manuscript.

Funding: M.D., J.P. and J.S. thank GACR project 21-06825X for the support and institutional support from RVO:67985815. The work of L.M. and F.M. is partially supported by the PRIN grant 2022LWPEXW of the Italian Ministry of University and Research (MUR). H.K. and N.R.C. acknowledge NASA funding through the grants 80NSSC20K0329, 80NSSC21K1817, 80NSSC22K1291, 80NSSC22K1883, 80NSSC23K1041, 80NSSC24K0205, and 80NSSC24K1178, as well as support by the McDonnell Center for the Space Sciences at Washington University. N.R.C. acknowledges support by the John Templeton Foundation. G.M. acknowledges financial support of the Marie Skłodowska-Curie grant agreement No. 101107057.

Data Availability Statement: *IXPE* observations are public and can be freely downloaded and reduced here: https://heasarc.gsfc.nasa.gov/docs/ixpe/archive accessed on 24 September 2024.

Acknowledgments: We thank the IXPE mission operations staff for their effort and dedication in planning the ToOs and DDTs for BH XRB observations. Our special thanks go to the original mission PI, Martin Weisskopf, for leadership of the *IXPE* mission, Allyn Tennant and the IXPE operations team for their invaluable work in ToO execution, Luca Baldini for his help with all aspects of `ixpeobssim`, and to Keith Arnaud for all his help in polarisation implementation into `xspec`. M.D. would like to thank all the active members of the *IXPE* topical working group (TWG) of "Accreting Stellar-Mass Black Holes", especially to the leaders of these TWG observations, for very efficient collaboration and many fruitful discussions. The *Imaging X ray Polarimetry Explorer* (*IXPE*) is a joint US and Italian mission. The US contribution is supported by the National Aeronautics and Space Administration (NASA) and led and managed by its Marshall Space Flight Center (MSFC), with industry partner Ball Aerospace (contract NNM15AA18C). The Italian contribution is supported by the Italian Space Agency (Agenzia Spaziale Italiana, ASI) through contract ASI-OHBI-2022-13-I.0, agreements ASI-INAF-2022-19-HH.0 and ASI-INFN-2017.13-H0, and its Space Science Data Center (SSDC) with agreements ASI-INAF-2022-14-HH.0 and ASI-INFN 2021-43-HH.0, and by the Istituto Nazionale di Astrofisica (INAF) and the Istituto Nazionale di Fisica Nucleare (INFN) in Italy. This research used data products provided by the *IXPE* Team (MSFC, SSDC, INAF, and INFN) and

distributed with additional software tools by the High Energy Astrophysics Science Archive Research Center (HEASARC), at NASA Goddard Space Flight Center (GSFC). This research has made use of MAXI data provided by RIKEN, JAXA, and the MAXI team.

Conflicts of Interest: The authors declare no conflict of interest.

Abbreviations

The following abbreviations are used in this manuscript:

NASA	The National Aeronautics and Space Administration
ASI	Agenzia Spaziale Italiana
HEASARC	High Energy Astrophysics Science Archive Research Center
IXPE	Imaging X-ray Polarimetry Explorer
OSO	Orbiting Solar Observatory
NICER	Neutron star Interior Composition Explorer
NuSTAR	Nuclear Spectroscopic Telescope Array
XRISM	X-ray Imaging and Spectroscopy Mission
INTEGRAL	INTErnational Gamma-Ray Astrophysics Laboratory
MAXI	Monitor of All-sky X-ray Image
ATCA	Australia Telescope Compact Array
XPoSat	X-ray Polarimeter Satellite
POLIX	Polarimeter Instrument in X-rays
COSI	Compton Spectrometer and Imager
REDSoX	Rocket Experiment Demonstration of a Soft X-ray Polarimeter
FoV	Field of view
PD	Polarisation degree
PA	Polarisation angle
GO	General Observer
ToO	Target of Opportunity
DDT	Director's Discretionary Time
AGN	Active galactic nuclei
BH	Black hole
XRB	X-ray binary
LMXB	Low-mass X-ray binary
HMXB	High-mass X-ray binary
BHC	Black hole candidate
SS	Soft state
HS	Hard state
SPL	Steep power-law
IMS	Intermediate state
HIMS	Hard intermediate state
SIMS	Soft intermediate state
HID	Hardness-intensity diagram
TWG	Topical working group

Notes

1 Many of these still lack a proper mass measurement and thus are considered to be black hole candidates (BHC). Their nature is then derived from their spectral and timing characteristics.

2 Note that for polarisation degree of the order of 1%, the polarised flux is 100 times smaller than the total flux. Furthermore, the polarised flux needs to be measured in the presence of the statistical fluctuations of the unpolarised flux. Polarisation measurements thus need to be several orders of magnitude longer than flux measurements, assuming similar detector efficiencies. Additionally, the Gas Pixel Detector used in *IXPE* has lower efficiency than a typical CCD chip used in instruments for X-ray spectral observations.

3 See also the *Note on IXPE Statistics* prepared by the *IXPE* team at https://heasarc.gsfc.nasa.gov/docs/ixpe/analysis/IXPE_Stats-Advice.pdf accessed on 24 September 2024.

4 Since the BH XRBs are usually point source objects, the *IXPE* imaging capabilities have been used only once for these types of targets – for the eastern lobe of SS 433. Note that imaging has been used to its full potential in other extended objects like

supernova remnants, pulsar wind nebulae, clouds in Sgr A*, and others. Notwithstanding, imaging capabilities provide a strong background reduction for some of the observed targets that were relatively faint.

[5] See https://heasarc.gsfc.nasa.gov/docs/ixpe/archive/ accessed on 24 September 2024.

[6] The `ixpecalcarf` exits with an error message "The attitude file contains 100.0% of off-axis angle(s) larger than the maximum value in the vignetting CALDB file."

[7] The best approach would be to use the forward folding method, i.e., fitting a model to all three Stokes parameters. However, this would be too demanding and is beyond the scope of this review, where we seek a simple, uniform approach. When our results are compared with those obtained using the forward folding method, e.g., for Swift J1727.8–1613 in [39], we find excellent agreement well within statistical errors.

[8] To check all the details on the source state, we refer the reader to the original *IXPE* team papers on these observations.

[9] Note that the SS in Cyg X–1 is not quite like the SS in other BH XRB sources because the Compton component tends to be much stronger, see, e.g., [61].

[10] Taking the mass accretion rate of 0.22×10^{18} g/s and spin $a = 0.96$, as in [38], gives the accretion rate to be 0.015 in Eddington units. This is an order of magnitude smaller than an accretion rate in a typical SS of other BH XRBs. Note also that, according to [38], the spectrum above 4 keV is dominated by coronal Comptonised radiation and its reflection from the accretion disc, contrary to the typical SS, where the dominance of the thermal emission is much more prominent.

[11] See https://www.isro.gov.in/XPoSat.html accessed on 24 September 2024.

References

1. Tetarenko, B.E.; Sivakoff, G.R.; Heinke, C.O.; Gladstone, J.C. WATCHDOG: A Comprehensive All-sky Database of Galactic Black Hole X-ray Binaries. *Astrophys. J. Suppl.* **2016**, *222*, 15. [CrossRef]
2. Corral-Santana, J.M.; Casares, J.; Muñoz-Darias, T.; Bauer, F.E.; Martínez-Pais, I.G.; Russell, D.M. BlackCAT: A catalogue of stellar-mass black holes in X-ray transients. *Astron. Astrophys.* **2016**, *587*, A61. [CrossRef]
3. Zdziarski, A.A.; Gierliński, M. Radiative Processes, Spectral States and Variability of Black-Hole Binaries. *Progr. Theor. Phys. Suppl.* **2004**, *155*, 99–119. [CrossRef]
4. Fender, R.P.; Belloni, T.M.; Gallo, E. Towards a unified model for black hole X-ray binary jets. *Mon. Not. R. Astron. Soc.* **2004**, *355*, 1105–1118. [CrossRef]
5. Done, C. Observational characteristics of accretion onto black holes. *arXiv* **2010**, arXiv:1008.2287. [CrossRef]
6. Shakura, N.I.; Sunyaev, R.A. Reprint of 1973A&A....24..337S. Black holes in binary systems. Observational appearance. *Astron. Astrophys.* **1973**, *500*, 33–51.
7. Novikov, I.D.; Thorne, K.S. Astrophysics of black holes. In Proceedings of the Black Holes (Les Astres Occlus), New York, NY, USA, 1973 ; pp. 343–450.
8. Maccarone, T.J. Do X-ray binary spectral state transition luminosities vary? *Astron. Astrophys.* **2003**, *409*, 697–706. [CrossRef]
9. McClintock, J.E.; Remillard, R.A. Black hole binaries. In *Compact Stellar X-ray Sources*; Lewin, W.H.G., van der Klis, M., Eds.; Cambridge Astrophysics Series; Cambridge University Press: Cambridge, UK, 2006; Volume 39, pp. 157–213. [CrossRef]
10. Middleton, M.J.; Walton, D.J.; Alston, W.; Dauser, T.; Eikenberry, S.; Jiang, Y.F.; Fabian, A.C.; Fuerst, F.; Brightman, M.; Marshall, H.; et al. NuSTAR reveals the hidden nature of SS433. *Mon. Not. R. Astron. Soc.* **2021**, *506*, 1045–1058. [CrossRef]
11. Poutanen, J.; Lipunova, G.; Fabrika, S.; Butkevich, A.G.; Abolmasov, P. Supercritically accreting stellar mass black holes as ultraluminous X-ray sources. *Mon. Not. R. Astron. Soc.* **2007**, *377*, 1187–1194. [CrossRef]
12. Sądowski, A.; Narayan, R.; McKinney, J.C.; Tchekhovskoy, A. Numerical simulations of super-critical black hole accretion flows in general relativity. *Mon. Not. R. Astron. Soc.* **2014**, *439*, 503–520. [CrossRef]
13. Koljonen, K.I.I.; Tomsick, J.A. The obscured X-ray binaries V404 Cyg, Cyg X–3, V4641 Sgr, and GRS 1915+105. *Astron. Astrophys.* **2020**, *639*, A13. [CrossRef]
14. Long, K.S.; Chanan, G.A.; Novick, R. The X-ray polarization of the CYG sources. *Astrophys. J.* **1980**, *238*, 710–716. [CrossRef]
15. Chauvin, M.; Roques, J.P.; Clark, D.J.; Jourdain, E. Polarimetry in the Hard X-Ray Domain with INTEGRAL SPI. *Astrophys. J.* **2013**, *769*, 137. [CrossRef]
16. Vadawale, S.V.; Chattopadhyay, T.; Rao, A.R.; Bhattacharya, D.; Bhalerao, V.B.; Vagshette, N.; Pawar, P.; Sreekumar, S. Hard X-ray polarimetry with Astrosat-CZTI. *Astron. Astrophys.* **2015**, *578*, A73. [CrossRef]
17. Connors, P.A.; Stark, R.F. Observable gravitational effects on polarised radiation coming from near a black hole. *Nature* **1977**, *269*, 128–129. [CrossRef]
18. Connors, P.A.; Piran, T.; Stark, R.F. Polarization features of X-ray radiation emitted near black holes. *Astrophys. J.* **1980**, *235*, 224–244. [CrossRef]
19. Dovčiak, M.; Muleri, F.; Goosmann, R.W.; Karas, V.; Matt, G. Thermal disc emission from a rotating black hole: X-ray polarization signatures. *Mon. Not. R. Astron. Soc.* **2008**, *391*, 32–38. [CrossRef]
20. Schnittman, J.D.; Krolik, J.H. X-ray Polarization from Accreting Black Holes: The Thermal State. *Astrophys. J.* **2009**, *701*, 1175–1187. [CrossRef]
21. Schnittman, J.D.; Krolik, J.H. X-ray Polarization from Accreting Black Holes: Coronal Emission. *Astrophys. J.* **2010**, *712*, 908–924. [CrossRef]

22. Krawczynski, H.; Beheshtipour, B. New Constraints on the Spin of the Black Hole Cygnus X–1 and the Physical Properties of its Accretion Disk Corona. *Astrophys. J.* **2022**, *934*, 4. [CrossRef]
23. Zhang, W.; Dovčiak, M.; Bursa, M.; Karas, V.; Matt, G.; Ursini, F. Investigating the X-ray polarization of lamp-post coronae in BHXRBs. *Mon. Not. R. Astron. Soc.* **2022**, *515*, 2882–2889. [CrossRef]
24. Weisskopf, M.C.; Soffitta, P.; Baldini, L.; Ramsey, B.D.; O'Dell, S.L.; Romani, R.W.; Matt, G.; Deininger, W.D.; Baumgartner, W.H.; Bellazzini, R.; et al. The Imaging X-Ray Polarimetry Explorer (IXPE): Pre-Launch. *J. Astron. Telesc. Instruments, Syst.* **2022**, *8*, 026002. [CrossRef]
25. Kaaret, P.; Ferrazzoli, R.; Silvestri, S.; Negro, M.; Manfreda, A.; Wu, K.; Costa, E.; Soffitta, P.; Safi-Harb, S.; Poutanen, J.; et al. X-Ray Polarization of the Eastern Lobe of SS 433. *Astrophys. J. Lett.* **2024**, *961*, L12. [CrossRef]
26. Bardeen, J.M.; Press, W.H.; Teukolsky, S.A. Rotating Black Holes: Locally Nonrotating Frames, Energy Extraction, and Scalar Synchrotron Radiation. *Astrophys. J.* **1972**, *178*, 347–370. [CrossRef]
27. Mellinger, A. A Color All-Sky Panorama Image of the Milky Way. *Publ. Astron. Soc. Pac.* **2009**, *121*, 1180. [CrossRef]
28. Gendreau, K.C.; Arzoumanian, Z.; Okajima, T. The Neutron star Interior Composition ExploreR (NICER): An Explorer mission of opportunity for soft x-ray timing spectroscopy. In Proceedings of the Space Telescopes and Instrumentation 2012: Ultraviolet to Gamma Ray, Amsterdam, The Netherlands, 1–6 July 2012 ; Takahashi, T.; Murray, S.S., den Herder, J.W.A., Eds.; SPIE: Bellingham,WA, USA, 2012; Volume 8443, p. 844313. [CrossRef]
29. Harrison, F.A.; Craig, W.W.; Christensen, F.E.; Hailey, C.J.; Zhang, W.W.; Boggs, S.E.; Stern, D.; Cook, W.R.; Forster, K.; Giommi, P.; et al. The Nuclear Spectroscopic Telescope Array (NuSTAR) High-energy X-Ray Mission. *Astrophys. J.* **2013**, *770*, 103. [CrossRef]
30. Tashiro, M.; Maejima, H.; Toda, K.; Kelley, R.; Reichenthal, L.; Hartz, L.; Petre, R.; Williams, B.; Guainazzi, M.; Costantini, E.; et al. Status of x-ray imaging and spectroscopy mission (XRISM). In Proceedings of the Space Telescopes and Instrumentation 2020: Ultraviolet to Gamma Ray, Online, 14–18 December 2020; Society of Photo-Optical Instrumentation Engineers (SPIE) Conference Series; den Herder, J.W.A., Nikzad, S., Nakazawa, K., Eds.; SPIE: Bellingham,WA, USA, 2020; Volume 11444, p. 1144422. [CrossRef]
31. Winkler, C.; Courvoisier, T.J.L.; Di Cocco, G.; Gehrels, N.; Giménez, A.; Grebenev, S.; Hermsen, W.; Mas-Hesse, J.M.; Lebrun, F.; Lund, N.; et al. The INTEGRAL mission. *Astron. Astrophys.* **2003**, *411*, L1–L6. [CrossRef]
32. Gehrels, N.; Chincarini, G.; Giommi, P.; Mason, K.O.; Nousek, J.A.; Wells, A.A.; White, N.E.; Barthelmy, S.D.; Burrows, D.N.; Cominsky, L.R.; et al. The Swift Gamma-Ray Burst Mission. *Astrophys. J.* **2004**, *611*, 1005–1020. [CrossRef]
33. Matsuoka, M.; Kawasaki, K.; Ueno, S.; Tomida, H.; Kohama, M.; Suzuki, M.; Adachi, Y.; Ishikawa, M.; Mihara, T.; Sugizaki, M.; et al. The MAXI Mission on the ISS: Science and Instruments for Monitoring All-Sky X-Ray Images. *Publ. Astron. Soc. Jpn.* **2009**, *61*, 999. [CrossRef]
34. Baldini, L.; Bucciantini, N.; Lalla, N.D.; Ehlert, S.; Manfreda, A.; Negro, M.; Omodei, N.; Pesce-Rollins, M.; Sgrò, C.; Silvestri, S. ixpeobssim: A simulation and analysis framework for the imaging X-ray polarimetry explorer. *SoftwareX* **2022**, *19*, 101194. [CrossRef]
35. Arnaud, K.A. XSPEC: The First Ten Years. In Proceedings of the Astronomical Data Analysis Software and Systems V, Tucson, Arizona, 23–25 October 1995; Astronomical Society of the Pacific Conference Series; Jacoby, G.H., Barnes, J., Eds.; Astronomical Society of the Pacific: San Francisco, CA, USA, 1996; Volume 101, pp. 17–20.
36. Di Marco, A.; Soffitta, P.; Costa, E.; Ferrazzoli, R.; La Monaca, F.; Rankin, J.; Ratheesh, A.; Xie, F.; Baldini, L.; Del Monte, E.; et al. Handling the Background in IXPE Polarimetric Data. *Astron. J.* **2023**, *165*, 143. [CrossRef]
37. Krawczynski, H.; Muleri, F.; Dovčiak, M.; Veledina, A.; Rodriguez Cavero, N.; Svoboda, J.; Ingram, A.; Matt, G.; Garcia, J.A.; Loktev, V.; et al. Polarized x-rays constrain the disk-jet geometry in the black hole x-ray binary Cygnus X–1. *Science* **2022**, *378*, 650–654. [CrossRef] [PubMed]
38. Steiner, J.F.; Nathan, E.; Hu, K.; Krawczynski, H.; Dovčiak, M.; Veledina, A.; Muleri, F.; Svoboda, J.; Alabarta, K.; Parra, M.; et al. An IXPE-led X-Ray Spectropolarimetric Campaign on the Soft State of Cygnus X–1: X-Ray Polarimetric Evidence for Strong Gravitational Lensing. *Astrophys. J. Lett.* **2024**, *969*, L30. [CrossRef]
39. Ingram, A.; Bollemeijer, N.; Veledina, A.; Dovciak, M.; Poutanen, J.; Egron, E.; Russell, T.D.; Trushkin, S.A.; Negro, M.; Ratheesh, A.; et al. Tracking the X-ray Polarization of the Black Hole Transient Swift J1727.8–1613 during a State Transition. *Astrophys. J.* **2024**, *968*, 76. [CrossRef]
40. Simmons, J.F.L.; Stewart, B.G. Point and interval estimation of the true unbiased degree of linear polarization in the presence of low signal-to-noise ratios. *Astron. Astrophys.* **1985**, *142*, 100–106.
41. Stewart, B.G. Polynomial FITS for Polarization Estimation. *Astron. Astrophys.* **1991**, *246*, 280.
42. Maier, D.; Tenzer, C.; Santangelo, A. Point and Interval Estimation on the Degree and the Angle of Polarization: A Bayesian Approach. *Publ. Astron. Soc. Pac.* **2014**, *126*, 459. [CrossRef]
43. Mastroserio, G.; De Marco, B.; Baglio, M.C.; Carotenuto, F.; Fabiani, S.; Russell, T.D.; Capitanio, F.; Cavecchi, Y.; Motta, S.; Russell, D.M.; et al. X-ray and optical polarization aligned with the radio jet ejecta in GX 339–4. *arXiv* **2024**, arXiv:2408.06856. [CrossRef]
44. Rodriguez Cavero, N. First Year of Stellar-Mass Black Hole Observations with the Imaging X-ray Polarimetry Explorer. *arXiv* **2024**, arXiv:2402.10371. [CrossRef]
45. Veledina, A.; Muleri, F.; Poutanen, J.; Podgorný, J.; Dovčiak, M.; Capitanio, F.; Churazov, E.; De Rosa, A.; Di Marco, A.; Forsblom, S.V.; et al. Cygnus X–3 revealed as a Galactic ultraluminous X-ray source by IXPE. *Nat. Astron.* **2024**, 8, 1031–1046. [CrossRef]

46. Veledina, A.; Poutanen, J.; Bocharova, A.; Di Marco, A.; Forsblom, S.V.; La Monaca, F.; Podgorny, J.; Tsygankov, S.S.; Zdziarski, A.A.; Ahlberg, V.; et al. Ultrasoft state of microquasar Cygnus X–3: X-ray polarimetry reveals the geometry of astronomical puzzle. *Astron. Astrophys.* **2024**, *688*, L27. [CrossRef]
47. Podgorný, J.; Marra, L.; Muleri, F.; Rodriguez Cavero, N.; Ratheesh, A.; Dovčiak, M.; Mikušincová, R.; Brigitte, M.; Steiner, J.F.; Veledina, A.; et al. The first X-ray polarimetric observation of the black hole binary LMC X–1. *Mon. Not. R. Astron. Soc.* **2023**. [CrossRef]
48. Svoboda, J.; Dovčiak, M.; Steiner, J.F.; Muleri, F.; Ingram, A.; Yilmaz, A.; Rodriguez Cavero, N.; Marra, L.; Poutanen, J.; Veledina, A.; et al. First X-Ray Polarization Measurement Confirms the Low Black Hole Spin in LMC X–3. *Astrophys. J.* **2024**, *960*, 3. [CrossRef]
49. Marra, L.; Brigitte, M.; Rodriguez Cavero, N.; Chun, S.; Steiner, J.F.; Dovčiak, M.; Nowak, M.; Bianchi, S.; Capitanio, F.; Ingram, A.; et al. IXPE observation confirms a high spin value in the accreting black hole 4U 1957+115. *Astron. Astrophys.* **2024**, *684*, A95. [CrossRef]
50. Ratheesh, A.; Dovčiak, M.; Krawczynski, H.; Podgorný, J.; Marra, L.; Veledina, A.; Suleimanov, V.; Rodriguez Cavero, N.; Steiner, J.; Svoboda, J.; et al. The high polarisation of the X-rays from the Black Hole X-ray Binary 4U 1630–47 challenges standard thin accretion disc scenario. *Astrophys. J.* **2024**, *964*, 77. [CrossRef]
51. Rodriguez Cavero, N.; Marra, L.; Krawczynski, H.; Dovčiak, M.; Bianchi, S.; Steiner, J.F.; Svoboda, J.; Capitanio, F.; Matt, G.; Negro, M.; et al. The First X-Ray Polarization Observation of the Black Hole X-Ray Binary 4U 1630–47 in the Steep Power-law State. *Astrophys. J. Lett.* **2023**, *958*, L8. [CrossRef]
52. Veledina, A.; Muleri, F.; Dovčiak, M.; Poutanen, J.; Ratheesh, A.; Capitanio, F.; Matt, G.; Soffitta, P.; Tennant, A.F.; Negro, M.; et al. Discovery of X-Ray Polarization from the Black Hole Transient Swift J1727.8–1613. *Astrophys. J. Lett.* **2023**, *958*, L16. [CrossRef]
53. Svoboda, J.; Dovčiak, M.; Steiner, J.F.; Kaaret, P.; Podgorný, J.; Poutanen, J.; Veledina, A.; Muleri, F.; Taverna, R.; Krawczynski, H.; et al. Dramatic Drop in the X-Ray Polarization of Swift J1727.8–1613 in the Soft Spectral State. *Astrophys. J. Lett.* **2024**, *966*, L35. [CrossRef]
54. Podgorný, J.; Svoboda, J.; Dovčiak, M.; Veledina, A.; Poutanen, J.; Kaaret, P.; Bianchi, S.; Ingram, A.; Capitanio, F.; Datta, S.R.; et al. Recovery of the X-ray polarisation of Swift J1727.8–1613 after the soft-to-hard spectral transition. *Astron. Astrophys.* **2024**, *686*, L12. [CrossRef]
55. Miller-Jones, J.C.A.; Bahramian, A.; Orosz, J.A.; Mandel, I.; Gou, L.; Maccarone, T.J.; Neijssel, C.J.; Zhao, X.; Ziółkowski, J.; Reid, M.J.; et al. Cygnus X–1 contains a 21-solar mass black hole—Implications for massive star winds. *Science* **2021**, *371*, 1046–1049. [CrossRef]
56. Orosz, J.A.; McClintock, J.E.; Aufdenberg, J.P.; Remillard, R.A.; Reid, M.J.; Narayan, R.; Gou, L. The Mass of the Black Hole in Cygnus X–1. *Astrophys. J.* **2011**, *742*, 84. [CrossRef]
57. Gou, L.; McClintock, J.E.; Remillard, R.A.; Steiner, J.F.; Reid, M.J.; Orosz, J.A.; Narayan, R.; Hanke, M.; García, J. Confirmation via the Continuum-fitting Method that the Spin of the Black Hole in Cygnus X–1 Is Extreme. *Astrophys. J.* **2014**, *790*, 29. [CrossRef]
58. Tomsick, J.A.; Nowak, M.A.; Parker, M.; Miller, J.M.; Fabian, A.C.; Harrison, F.A.; Bachetti, M.; Barret, D.; Boggs, S.E.; Christensen, F.E.; et al. The Reflection Component from Cygnus X–1 in the Soft State Measured by NuSTAR and Suzaku. *Astrophys. J.* **2014**, *780*, 78. [CrossRef]
59. Poutanen, J.; Veledina, A.; Beloborodov, A.M. Polarized X-Rays from Windy Accretion in Cygnus X–1. *Astrophys. J. Lett.* **2023**, *949*, L10. [CrossRef]
60. Dexter, J.; Begelman, M.C. A relativistic outflow model of the X-ray polarization in Cyg X–1. *Mon. Not. R. Astron. Soc.* **2024**, *528*, L157–L160. [CrossRef]
61. Remillard, R.A.; McClintock, J.E. X-Ray Properties of Black-Hole Binaries. *Annu. Rev. Astron. Astrophys.* **2006**, *44*, 49–92. [CrossRef]
62. Dovciak, M.; Steiner, J.F.; Krawczynski, H.; Svoboda, J. First Results of IXPE X-ray Polarization Measurements of Cyg X–1 in its Soft State. *Astron. Telegr.* **2023**, *16084*, 1.
63. Jana, A.; Chang, H.K. X-ray polarization changes with the state transition in Cygnus X–1. *Mon. Not. R. Astron. Soc.* **2024**, *527*, 10837–10843. [CrossRef]
64. Reid, M.J.; Miller-Jones, J.C.A. On the Distances to the X-Ray Binaries Cygnus X–3 and GRS 1915+105. *Astrophys. J.* **2023**, *959*, 85. [CrossRef]
65. Koljonen, K.I.I.; Maccarone, T.J. Gemini/GNIRS infrared spectroscopy of the Wolf-Rayet stellar wind in Cygnus X–3. *Mon. Not. R. Astron. Soc.* **2017**, *472*, 2181–2195. [CrossRef]
66. Zdziarski, A.A.; Mikolajewska, J.; Belczynski, K. Cyg X–3: A low-mass black hole or a neutron star. *Mon. Not. R. Astron. Soc.* **2013**, *429*, L104–L108. [CrossRef]
67. van Kerkwijk, M.H.; Charles, P.A.; Geballe, T.R.; King, D.L.; Miley, G.K.; Molnar, L.A.; van den Heuvel, E.P.J.; van der Klis, M.; van Paradijs, J. Infrared helium emission lines from Cygnus X–3 suggesting a Wolf-Rayet star companion. *Nature* **1992**, *355*, 703–705. [CrossRef]
68. Martí, J.; Paredes, J.M.; Peracaula, M. The Cygnus X–3 Radio Jets at Arcsecond Scales. *Astrophys. J.* **2000**, *545*, 939–944. [CrossRef]
69. Antokhin, I.I.; Cherepashchuk, A.M.; Antokhina, E.A.; Tatarnikov, A.M. Near-IR and X-Ray Variability of Cyg X–3: Evidence for a Compact IR Source and Complex Wind Structures. *Astrophys. J.* **2022**, *926*, 123. [CrossRef]

70. Pietrzyński, G.; Graczyk, D.; Gieren, W.; Thompson, I.B.; Pilecki, B.; Udalski, A.; Soszyński, I.; Kozłowski, S.; Konorski, P.; Suchomska, K.; et al. An eclipsing-binary distance to the Large Magellanic Cloud accurate to two per cent. *Nature* **2013**, *495*, 76–79. [CrossRef] [PubMed]
71. Orosz, J.A.; Steeghs, D.; McClintock, J.E.; Torres, M.A.P.; Bochkov, I.; Gou, L.; Narayan, R.; Blaschak, M.; Levine, A.M.; Remillard, R.A.; et al. A New Dynamical Model for the Black Hole Binary LMC X–1. *Astrophys. J.* **2009**, *697*, 573–591. [CrossRef]
72. Gou, L.; McClintock, J.E.; Liu, J.; Narayan, R.; Steiner, J.F.; Remillard, R.A.; Orosz, J.A.; Davis, S.W.; Ebisawa, K.; Schlegel, E.M. A DETERMINATION OF THE SPIN OF THE BLACK HOLE PRIMARY IN LMC X–1. *Astrophys. J.* **2009**, *701*, 1076. [CrossRef]
73. Steiner, J.F.; Reis, R.C.; Fabian, A.C.; Remillard, R.A.; McClintock, J.E.; Gou, L.; Cooke, R.; Brenneman, L.W.; Sanders, J.S. A broad iron line in LMC X–1. *Mon. Not. R. Astron. Soc.* **2012**, *427*, 2552–2561. [CrossRef]
74. Majumder, S.; Kushwaha, A.; Das, S.; Nandi, A. First detection of X-ray polarization in thermal state of LMC X–3: Spectro-polarimetric study with IXPE. *Mon. Not. R. Astron. Soc.* **2024**, *527*, L76–L81. [CrossRef]
75. Garg, A.; Rawat, D.; Méndez, M. Unveiling the X-ray polarimetric properties of LMC X–3 with IXPE, NICER, and Swift/XRT. *Mon. Not. R. Astron. Soc.* **2024**, *531*, 585–591. [CrossRef]
76. Orosz, J.A.; Steiner, J.F.; McClintock, J.E.; Buxton, M.M.; Bailyn, C.D.; Steeghs, D.; Guberman, A.; Torres, M.A.P. The Mass of the Black Hole in LMC X–3. *Astrophys. J.* **2014**, *794*, 154. [CrossRef]
77. Steiner, J.F.; McClintock, J.E.; Orosz, J.A.; Remillard, R.A.; Bailyn, C.D.; Kolehmainen, M.; Straub, O. The Low-spin Black Hole in LMC X–3. *Astrophys. J. Lett.* **2014**, *793*, L29. [CrossRef]
78. Yilmaz, A.; Svoboda, J.; Grinberg, V.; Boorman, P.G.; Bursa, M.; Dovčiak, M. Accretion disc evolution in GRO J1655–40 and LMC X–3 with relativistic and non-relativistic disc models. *Mon. Not. R. Astron. Soc.* **2023**, *525*, 1288–1310. [CrossRef]
79. Mikusincova, R.; Dovciak, M.; Bursa, M.; Lalla, N.D.; Matt, G.; Svoboda, J.; Taverna, R.; Zhang, W. X-ray polarimetry as a tool to measure the black hole spin in microquasars: Simulations of IXPE capabilities. *Mon. Not. R. Astron. Soc.* **2023**, *519*, 6138–6148. [CrossRef]
80. Rawat, D.; Garg, A.; Méndez, M. Spectropolarimetric study of 4U 1630–47 in steep power-law state with IXPE and NICER. *Mon. Not. R. Astron. Soc.* **2023**, *525*, 661–666. [CrossRef]
81. Kushwaha, A.; Jayasurya, K.M.; Agrawal, V.K.; Nandi, A. IXPE and NICER view of black hole X-ray binary 4U 1630–47: First significant detection of polarized emission in thermal state. *Mon. Not. R. Astron. Soc.* **2023**, *524*, L15–L20. [CrossRef]
82. Rawat, D.; Garg, A.; Méndez, M. Detection of X-Ray Polarized Emission and Accretion-disk Winds with IXPE and NICER in the Black Hole X-Ray Binary 4U 1630–47. *Astrophys. J. Lett.* **2023**, *949*, L43. [CrossRef]
83. West, A.T.; Krawczynski, H. Impact of the Accretion Disk Thickness on the Polarization of the Thermal Emission from Stellar Mass Black Holes. *Astrophys. J.* **2023**, *957*, 9. [CrossRef]
84. Tomaru, R.; Done, C.; Odaka, H. X-ray polarization properties of thermal-radiative disc winds in binary systems. *Mon. Not. R. Astron. Soc.* **2024**, *527*, 7047–7054. [CrossRef]
85. Ratheesh, A.; Matt, G.; Tombesi, F.; Soffitta, P.; Pesce-Rollins, M.; Di Marco, A. Exploring the accretion-ejection geometry of GRS 1915+105 in the obscured state with future X-ray spectro-polarimetry. *Astron. Astrophys.* **2021**, *655*, A96. [CrossRef]
86. Kennea, J.A.; Swift Team. GRB 230824A is likely a Galactic Transient: Swift J1727.8–1613. *GRB Coord. Netw.* **2023**, *34540*, 1.
87. Negoro, H.; Serino, M.; Nakajima, M.; Kobayashi, K.; Tanaka, M.; Soejima, Y.; Kudo, Y.; Mihara, T.; Kawamuro, T.; Yamada, S.; et al. MAXI/GSC detection of Swift J1727.8–1613 (GRB 230824A). *GRB Coord. Netw.* **2023**, *34544*, 1.
88. Mata Sánchez, D.; Muñoz-Darias, T.; Armas Padilla, M.; Casares, J.; Torres, M.A.P. Evidence for inflows and outflows in the nearby black hole transient Swift J1727.8−162. *Astron. Astrophys.* **2024**, *682*, L1. [CrossRef]
89. Peng, J.Q.; Zhang, S.; Shui, Q.C.; Zhang, S.N.; Kong, L.D.; Chen, Y.P.; Wang, P.J.; Ji, L.; Qu, J.L.; Tao, L.; et al. NICER, NuSTAR, and Insight-HXMT Views to the Newly Discovered Black Hole X-Ray Binary Swift J1727.8–1613. *Astrophys. J. Lett.* **2024**, *960*, L17. [CrossRef]
90. Wood, C.M.; Miller-Jones, J.C.A.; Bahramian, A.; Tingay, S.J.; Prabu, S.; Russell, T.D.; Atri, P.; Carotenuto, F.; Altamirano, D.; Motta, S.E.; et al. Swift J1727.8–1613 has the Largest Resolved Continuous Jet Ever Seen in an X-ray Binary. *Astrophys. J. Lett.* **2024**, *971*, L9. [CrossRef]
91. Zhao, Q.C.; Tao, L.; Li, H.C.; Zhang, S.N.; Feng, H.; Ge, M.Y.; Ji, L.; Wang, Y.N.; Huang, Y.; Ma, X.; et al. The First Polarimetric View on Quasiperiodic Oscillations in a Black Hole X-Ray Binary. *Astrophys. J. Lett.* **2024**, *961*, L42. [CrossRef]
92. Zdziarski, A.A.; Ziółkowski, J.; Mikołajewska, J. The X-ray binary GX 339–4/V821 Ara: The distance, inclination, evolutionary status, and mass transfer. *Mon. Not. R. Astron. Soc.* **2019**, *488*, 1026–1034. [CrossRef]
93. Miller, J.M.; Fabian, A.C.; Reynolds, C.S.; Nowak, M.A.; Homan, J.; Freyberg, M.J.; Ehle, M.; Belloni, T.; Wijnands, R.; van der Klis, M.; et al. Evidence of Black Hole Spin in GX 339–4: XMM-Newton/EPIC-pn and RXTE Spectroscopy of the Very High State. *Astrophys. J. Lett.* **2004**, *606*, L131–L134. [CrossRef]
94. García, J.A.; Steiner, J.F.; McClintock, J.E.; Remillard, R.A.; Grinberg, V.; Dauser, T. X-Ray Reflection Spectroscopy of the Black Hole GX 339–4: Exploring the Hard State with Unprecedented Sensitivity. *Astrophys. J.* **2015**, *813*, 84. [CrossRef]
95. Ludlam, R.M.; Miller, J.M.; Cackett, E.M. Reapproaching the Spin Estimate of GX 339–4. *Astrophys. J.* **2015**, *806*, 262. [CrossRef]
96. Kolehmainen, M.; Done, C.; Díaz Trigo, M. Modelling the high-mass accretion rate spectra of GX 339–4: Black hole spin from reflection? *Mon. Not. R. Astron. Soc.* **2011**, *416*, 311–321. [CrossRef]
97. Yamada, S.; Makishima, K.; Uehara, Y.; Nakazawa, K.; Takahashi, H.; Dotani, T.; Ueda, Y.; Ebisawa, K.; Kubota, A.; Gandhi, P. Is the Black Hole in GX 339–4 Really Spinning Rapidly? *Astrophys. J. Lett.* **2009**, *707*, L109–L113. [CrossRef]

98. Gallo, E.; Corbel, S.; Fender, R.P.; Maccarone, T.J.; Tzioumis, A.K. A transient large-scale relativistic radio jet from GX 339–4. *Mon. Not. R. Astron. Soc.* **2004**, *347*, L52–L56. [CrossRef]
99. Kennea, J.A.; Lien, A.Y.; D'Elia, V.; Melandri, A.; Page, K.L.; Siegel, M.H. Swift J151857.0–572147: Swift detection of a new galactic X-ray transient. *Astron. Telegr.* **2024**, *16500*, 1.
100. Del Santo, M.; Russell, T.D.; Marino, A.; Motta, S. Swift/XRT observation of Swift J151857.0–572147 indicates that the source likely made a transition to the soft state. *Astron. Telegr.* **2024**, *16519*, 1.
101. Burridge, B.J.; Miller-Jones, J.C.A.; Bahramian, A.; Prabu, S.; Carotenuto, F.; Russell, T.D.; Cowie, F.; Fender, R.P. An HI spectroscopic distance constraint on Swift J151857.0–572147. *Astron. Telegr.* **2024**, *16538*, 1.
102. Carotenuto, F.; Russell, T.D. ATCA detection of an extremely bright radio flare from Swift J151857.0–572147. *Astron. Telegr.* **2024**, *16518*, 1.
103. Bardeen, J.M.; Petterson, J.A. The Lense-Thirring Effect and Accretion Disks around Kerr Black Holes. *Astrophys. J. Lett.* **1975**, *195*, L65. [CrossRef]
104. Shapiro, S.L.; Lightman, A.P.; Eardley, D.M. A two-temperature accretion disk model for Cygnus X–1: Structure and spectrum. *Astrophys. J.* **1976**, *204*, 187–199. [CrossRef]
105. Gianolli, V.E.; Kim, D.E.; Bianchi, S.; Agís-González, B.; Madejski, G.; Marin, F.; Marinucci, A.; Matt, G.; Middei, R.; Petrucci, P.O.; et al. Uncovering the geometry of the hot X-ray corona in the Seyfert galaxy NGC 4151 with IXPE. *Mon. Not. R. Astron. Soc.* **2023**, *523*, 4468–4476. [CrossRef]
106. Gianolli, V.E.; Bianchi, S.; Kammoun, E.; Gnarini, A.; Marinucci, A.; Ursini, F.; Parra, M.; Tortosa, A.; De Rosa, A.; Kim, D.E.; et al. A second view on the X-ray polarization of NGC 4151 with IXPE. *arXiv* **2024**, arXiv:2407.17243. [CrossRef]
107. Ingram, A.; Ewing, M.; Marinucci, A.; Tagliacozzo, D.; Rosario, D.J.; Veledina, A.; Kim, D.E.; Marin, F.; Bianchi, S.; Poutanen, J.; et al. The X-ray polarization of the Seyfert 1 galaxy IC 4329A. *Mon. Not. R. Astron. Soc.* **2023**, *525*, 5437–5449. [CrossRef]
108. Marin, F.; Gianolli, V.E.; Ingram, A.; Kim, D.E.; Marinucci, A.; Tagliacozzo, D.; Ursini, F. An Examination of the Very First Polarimetric X-ray Observations of Radio-Quiet Active Galactic Nuclei. *Galaxies* **2024**, *12*, 35. [CrossRef]
109. Mirabel, I.F.; Rodriguez, L.F.; Cordier, B.; Paul, J.; Lebrun, F. A double-sided radio jet from the compact Galactic Centre annihilator 1E1740.7–2942. *Nature* **1992**, *358*, 215–217. [CrossRef]
110. Ursini, F.; Marinucci, A.; Matt, G.; Bianchi, S.; Marin, F.; Marshall, H.L.; Middei, R.; Poutanen, J.; Rogantini, D.; De Rosa, A.; et al. Mapping the circumnuclear regions of the Circinus galaxy with the Imaging X-ray Polarimetry Explorer. *Mon. Not. R. Astron. Soc.* **2023**, *519*, 50–58. [CrossRef]
111. Marin, F.; Marinucci, A.; Laurenti, M.; Kim, D.E.; Barnouin, T.; Di Marco, A.; Ursini, F.; Bianchi, S.; Ravi, S.; Marshall, H.L.; et al. X-ray polarization measurement of the gold standard of radio- quiet active galactic nuclei: NGC 1068. *Astron. Astrophys.* **2024**, *689*, A238. [CrossRef]
112. van der Klis, M. Rapid X-ray Variability. In *Compact Stellar X-ray Sources*; Cambridge Astrophysics Series; Lewin, W.H.G., van der Klis, M., Eds.; Cambridge University Press: Cambridge, UK, 2006; Volume 39, pp. 39–112.
113. Markoff, S.; Nowak, M.A.; Wilms, J. Going with the Flow: Can the Base of Jets Subsume the Role of Compact Accretion Disk Coronae? *Astrophys. J.* **2005**, *635*, 1203–1216. [CrossRef]
114. Kara, E.; Steiner, J.F.; Fabian, A.C.; Cackett, E.M.; Uttley, P.; Remillard, R.A.; Gendreau, K.C.; Arzoumanian, Z.; Altamirano, D.; Eikenberry, S.; et al. The corona contracts in a black-hole transient. *Nature* **2019**, *565*, 198–201. [CrossRef]
115. Abarr, Q.; Awaki, H.; Baring, M.G.; Bose, R.; De Geronimo, G.; Dowkontt, P.; Errando, M.; Guarino, V.; Hattori, K.; Hayashida, K.; et al. XL-Calibur—A second-generation balloon-borne hard X-ray polarimetry mission. *Astropart. Phys.* **2021**, *126*, 102529. [CrossRef]
116. Lazar, H.; Lowell, A.; Tomsick, J.; Sleator, C.; Zoglauer, A.; Beechert, J.; Boggs, S.; Gulick, H.; Hartmann, D.; Karwin, C.; et al. Soft gamma-ray polarimetry with COSI. In Proceedings of the AAS/High Energy Astrophysics Division, Pittsburgh, PA, USA, 13–17 March 2022; Volume 19, p. 204.05.
117. Marshall, H.; Heine, S.; Garner, A.; Masterson, R.; Guenther, M.; Heilmann, R.; Bongiorno, S.; Gullikson, E. The Rocket Experiment Demonstration of a Soft X-ray Polarimeter (REDSoX). In Proceedings of the Multifrequency Behaviour of High Energy Cosmic Sources XIV, Palermo, Italy, 12–17 June 2023; Sissa Medialab srl: Trieste, Italy, 2024; p. 76.